

# Inviscid Axisymmetrization of an Elliptical Vortex

P. Koumoutsakos\*

*Center for Turbulence Research, NASA Ames 202A-1, Moffett Field, California 94035*  
E-mail: petros@nas.nasa.gov

Received July 18, 1996; revised May 13, 1997

---

The inviscid evolution of elliptical, nonuniform vorticity distributions is studied computationally using a high resolution Lagrangian (vortex) method with minimal numerical dissipation. The simulations reveal that the vortices evolve, through a process of filamentation, to a configuration consisting of a vortex surrounded by weak filamentary structures. The shape of the final configuration depends on the profile of the initial vorticity distribution. For the same ellipticity, relatively smooth profiles evolve to axisymmetric vortical structures, whereas sharper initial vorticity distributions result in robust non-axisymmetric configurations. A systematic convergence study is conducted to establish the accuracy of the method for long time inviscid simulations. To further assess the issue of axisymmetrization we compare our results with related numerical and experimental studies. © 1997 Academic Press

*Key Words:* vortex methods; inviscid vortical flows; vorticity axisymmetrization.

---

## INTRODUCTION

The increased power of supercomputers and advancements in the developments of numerical schemes have provided us with an increased insight into the simulation of two-dimensional incompressible flows for a wide range of Reynolds numbers. However, a difficulty still exists in accurately simulating the very high Reynolds number or inviscid, long time behavior of vortical flows. Such flows are characterized by the progressive production of finer scales and increasingly complex structures thus demanding a respective increase in the number of computational elements necessary for their resolution.

\* Also at the Institute of Fluid Dynamics, ETH, CH-8092, Zurich, Switzerland.

The computational study of inviscid flows was initiated in 1931 by Rosenhead [26] who attempted to simulate the evolution of a vortex sheet using a small number of point vortices. Subsequent efforts using point and vortex blob methods (see [18] for a review) reproduced qualitatively some of the phenomena observed in inviscid vortical flows but the computational cost and the low order accuracy of such methods failed to provide us with satisfactory extended simulations of complex flows. In 1979 Zabusky *et al.* [30] introduced another Lagrangian scheme, the method of contour dynamics (see [24] for a review). These methods simulate the evolution of piecewise constant distributions of vorticity. They reduce the computational requirements by one dimension to the accurate tracking of solely the boundary of such vortical structures. However, the continuous development of finer structures limited the applicability of such methods to relatively simple flows. The baton was passed on to Eulerian schemes and more specifically to *pseudo-spectral* methods [9]. Pseudo-spectral simulations use a hyperviscosity operator ( $\nabla^{2n}$ , usually  $n = 2, 4$ ) to extend the range of inviscid energy cascade that can be achieved by a given resolution. Analysis by Jiménez [13] and simulations of two-dimensional vortex stripping and erosion of coherent structures, have demonstrated that hyperviscosity can introduce spurious vortex dynamics.

In order to alleviate some of the difficulties of contour dynamics, Dritschel [7] devised the method of *contour surgery* (CS). In this method the piecewise constant structure of the vorticity field is maintained but concise truncation of the developing small scale structures has allowed for extended simulations of complex inviscid flows. Self-consistency tests as well as comparisons with other numerical methods [17] have demonstrated the consistency of this approach. Some questions remain [24] regarding the accurate simulation of the dynamics of smooth vortical structures by a respective limited number of piecewise constant vorticity distribution.

Recently by exploiting the observation that the equations governing the evolution of the charge density for magnetically confined electron columns are isomorphic to the Euler equations governing the vorticity field, Driscoll and Fine [6], have conducted experiments in magnetically confined plasmas the results of which bear direct relevance to two-dimensional vortical flows.

The development of the above-mentioned experimental and computational methods have allowed us to obtain significant insight and quantitative information regarding the evolution of vortical flows at the inviscid limit. However, as discussed by Pullin [24], there are several issues that remain unresolved. One of those is the problem of the long time evolution of an initially noncircular smooth vorticity distributions and its asymptotic state, namely the problem of *axisymmetrization*. On a related study Melander, McWilliams, and Zabusky [21] (hereafter referred to as MMZ) used the pseudo-spectral method with hyperviscosity to conduct simulations of the inviscid evolution of a smooth elliptical vortex. They conducted simulations for about  $13T_p$  (where  $T_p = 4\pi/\omega_{\max}$ ) and they observed relaxation towards an axisymmetric configuration consisting of a circular core surrounded by a disk of weak vorticity, arguing that the resulting large scale structures are essentially unchanged by the hyperviscosity. Dritschel [7] using a high resolution CS algorithm examined the behaviour of a sharper initial vorticity profile, by approximating the elliptical vorticity field with an eight level piecewise constant vorticity distribution.

Simulations for about  $6T_p$  did not result in an axisymmetric configuration but appear to asymptote towards a compact elliptical vorticity distribution surrounded by weak filamentary structures. The experimental results of Driscoll and Fine [6] suggest that the occurrence and extent of axisymmetrization depend on the profile and the ellipticity of the initial vorticity distribution.

In an effort to complement the above research efforts and to provide some further insight into the phenomenon of axisymmetrization, this paper presents a high resolution Lagrangian method, capable of accurate long time simulations of the inviscid evolution of smooth vortical structures. Our scheme is based on the classical scheme of point vortex methods [26]. Smooth vortex blobs, introduced by Chorin [4], are used to relax some of the difficulties associated with computations using point vortices. The vorticity field is discretized onto a set of vortices/particles and the solution of the Euler equations reduces to the accurate tracking of their trajectories. In the past vortex methods had been considered mostly as a scheme to obtain a qualitative rather than quantitative description of the flow. The main drawbacks of the scheme have been its computational cost that scales squared with the number of computational elements and their lack of accuracy and numerical convergence.

In order to reduce the computational cost Christiansen [5] introduced the method of Cloud in Cell. However, this scheme introduces additional dissipation and eliminates some of the inherent advantages of grid-free vortex methods. The last decade has seen the development of innovative algorithms to reduce the quadratic cost of the method. The scheme of multipole expansions [10] allows for computations that scale in cost linearly with the number of elements. This scheme has been efficiently implemented allowing for high resolution simulations using hundreds of thousands or millions [16] of computational elements.

Besides the relatively small number of computational elements employed in several vortex blob simulations in the past, the lack of accuracy and convergence may be also attributed to the failure to recognize the grid distortion (such as wave breaking and filamentation in contour dynamics) inherent to Lagrangian methods. As computational elements adapt to the flow map strong velocity gradients may result in significant distortion of the computational grid. In vortex methods the computational elements are directly linked to the vorticity field and this distortion may lead to the generation of spurious vortical structures and the failure of the method to converge. This issue has rarely been addressed in the past in the context of two-dimensional vortex methods, although theoretical studies [11] have shown, as early as 18 years ago, that particle overlap is necessary for the convergence of smooth vortex methods. Here a consistent remeshing algorithm is implemented that allows for the adaptive introduction of computational elements to resolve the complex structures developing in inviscid flows, while ensuring the accuracy of the method and maintaining its adaptive, grid-free character.

The present scheme is an alternative to related simulations by hyperviscous pseudo-spectral methods and contour surgery as it allows for the simulations of continuous distributions of vorticity using a Lagrangian method with minimal dissipation. A convergence study, varying the numerical parameters, is conducted to assess the accuracy of the method.

The method is applied in the simulation of the evolution of initially elliptical vortices to study the phenomenon of axisymmetrization. We consider the evolution of two different profiles that have been considered by previous investigations [21, 7]. The two profiles have different vorticity gradients and their parallel study herein reveals that the initial distribution is crucial to the later development of a vorticity field. Both vortical structures evolve through a process of filamentation to a rather robust configuration. However, one vorticity distribution (studied first by MMZ [21]) relaxes to an axisymmetric configuration, whereas the second (corresponding to a similar profile, first studied by Dritschel [7]) asymptotes to a robust non-axisymmetric configuration. A series of diagnostics (vorticity contours and profiles, effective aspect ratio) help us describe the evolution of the vorticity field. Our results are in agreement with the experimental findings of Driscoll and Fine [6]. They have demonstrated this dependence of the asymptotic state of the vorticity field on the initial condition and have described the axisymmetrization process as the spatial analog of Landau damping.

The results of the present simulations may help us gain further insight in the phenomenon of axisymmetrization and assess issues such as the effect of hyperviscosity in pseudo-spectral simulations and the importance or not of approximating continuous vorticity distributions by piecewise constant vorticity profiles in CS simulations.

In Section 1 the governing equations and the numerical method are presented. In Section 2 the issue of Lagrangian grid distortion is addressed and a remeshing algorithm is presented. Section 3 describes the computation of diagnostics in the context of vortex methods and in Section 4 a convergence study is presented that assesses the accuracy of the present methodology. In Section 5 the method is applied to the simulation of the inviscid evolution of initially elliptical vortices. The results of the present simulations are compared with those from pertinent experimental and computational works and the phenomenon of axisymmetrization is discussed.

## 1. THE 2D EULER EQUATIONS—VORTEX METHODS

Two-dimensional incompressible unsteady flow of an inviscid fluid may be described by the vorticity transport equation as

$$\frac{\partial \boldsymbol{\omega}}{\partial t} + \mathbf{u} \cdot \nabla \boldsymbol{\omega} = 0, \quad (1a)$$

where  $\mathbf{u}(\mathbf{x}, t)$  is the velocity and  $\boldsymbol{\omega} = \omega \hat{\mathbf{e}}_z = \nabla \times \mathbf{u}$  is the vorticity. The initial vorticity field is given as  $\omega(\mathbf{x}, t = 0) = \omega_0(\mathbf{x})$  and at infinity we have

$$\mathbf{u}(\mathbf{x}) \rightarrow 0 \quad \text{as } |\mathbf{x}| \rightarrow \infty. \quad (1b)$$

Using the definition of the vorticity and the continuity ( $\nabla \cdot \mathbf{u} = 0$ ) it can be shown that  $\mathbf{u}$  is related to  $\boldsymbol{\omega}$  by the Poisson equation

$$\nabla^2 \mathbf{u} = -\nabla \times \boldsymbol{\omega}. \quad (2)$$

The present numerical method is based on the discretization of the above equations in a Lagrangian frame using particle (vortex) methods. The vorticity equation (Eq. (1)) may be expressed in a Lagrangian formulation by solving for the vorticity carrying fluid elements ( $\mathbf{x}_a$ ) based on the set of equations

$$\begin{aligned}\frac{d\mathbf{x}_a}{dt} &= \mathbf{u}(\mathbf{x}_a, t) \\ \frac{d\boldsymbol{\omega}}{dt} &= 0.\end{aligned}\tag{3}$$

The velocity field may be determined by the vorticity field using the Green's function formulation for the solution of Poisson's equation (Eq. (2)).

$$\mathbf{u}(\mathbf{x}_a) = -\frac{1}{2\pi} \int \mathbf{K}(\mathbf{x}_a - \mathbf{y}) \times \boldsymbol{\omega} d\mathbf{y},\tag{4}$$

where  $\mathbf{K}(\mathbf{z}) = \mathbf{z}/|\mathbf{z}|^2$ . The use of the Biot–Savart law to compute the velocity field guarantees the enforcement of the boundary condition at infinity (Eq. (1b)).

In vortex methods, the vorticity field is considered as a discrete sum of the individual vorticity fields of the particles, having core radius  $\varepsilon$ , strength  $\Gamma(t)$ , and an individual distribution of vorticity determined by the function  $\eta_\varepsilon$  so that

$$\boldsymbol{\omega}(\mathbf{x}, t) = \sum_{n=1}^N \Gamma_n(t) \eta_\varepsilon(\mathbf{x} - \mathbf{x}_n(t)).\tag{5}$$

When this expression for the vorticity is substituted in Eq. (4) the singular integral operator  $\mathbf{K}$  is convolved with the smooth function  $\eta_\varepsilon$  and is replaced by the smooth operator  $K_\varepsilon$  [4]. The integral is subsequently discretized using a quadrature having as quadrature points the locations of the particles. The error in the computation of the velocity and the vorticity field is a combination of the errors made by the smoothing of the Biot–Savart kernel and the discretization of the integral on the location of the particles

$$\text{Smoothing error} + \text{Discretization error} = \mathcal{O}(\varepsilon^m) + \mathcal{O}\left(\varepsilon \left(\frac{h}{\varepsilon}\right)^n\right),$$

where  $h$  is a characteristic distance between the particles and the exponents  $m, n$  depend on the properties of the smoothing function  $\eta_\varepsilon$ . For a table of smoothing functions along with their respective Biot–Savart kernels the reader is referred to Winckelmans and Leonard [28]. In the present study two smoothing functions are considered,

$$\text{Gaussian, } \eta_\varepsilon(\mathbf{x}) = \frac{1}{2\pi\varepsilon^2} e^{-|\mathbf{x}|/2\pi\varepsilon^2}$$

for which  $m = 2$  and  $n = \infty$  and

$$\text{super - Gaussian, } \eta_\varepsilon(\mathbf{x}) = \frac{1}{2\pi\varepsilon^2} \left( 2 - \frac{|\mathbf{x}|^2}{2} \right) e^{-|\mathbf{x}|^2/2\varepsilon^2}$$

for which  $m = 4$  and  $n = \infty$ .

Algorithmically the method may be expressed as

$$\begin{aligned} \frac{d\mathbf{x}_i}{dt} &= -\frac{1}{2\pi} \sum_{j=1}^N \Gamma_j K_\varepsilon(\mathbf{x}_i - \mathbf{x}_j) \quad \text{for } i = 1, \dots, N(t) \\ \frac{d\Gamma_i}{dt} &= 0 \quad \text{for } i = 1, \dots, N(t). \end{aligned} \tag{6}$$

Equation (3) has been replaced by a set of ODE's (Eq. (6)) whose solution is equivalent to the original set of equations. Note that the number of computational elements is a function of time, in order to maintain particle overlap as is discussed in the following sections.

### 1.1. Vectorization of Fast Vortex Methods—Computational Cost

The straightforward method of computing the right-hand side of Eq. (6) for every particle, requires  $\mathcal{O}(N^2)$  operations for  $N$  vortex elements. In the last decade fast methods have been developed that have operation counts of  $\mathcal{O}(N \log N)$  (“particle–box” method) or  $\mathcal{O}(N)$  (“box–box” method) [10], depending on the details of the algorithm. The basic idea of these methods is to decompose the element population spatially into clusters/boxes of particles and then build a hierarchy of clusters or a tree data structure—smaller neighboring clusters combine to form a cluster of the next size up in the hierarchy and so on.

The contribution of a cluster of particles to the velocity of a given vortex can then be computed to desired accuracy if the particle is sufficiently far from the cluster in proportion to the size of the cluster and a sufficiently large number of terms in the multipole expansion is taken. This is the essence of the “particle–box” method, requiring  $\mathcal{O}(N \log N)$  operations. One then tries to minimize the work required by maximizing the size of the cluster used while keeping the number of terms in the expansion within a reasonable limit and maintaining a certain degree of accuracy. The “box–box” scheme goes one step further as it accounts also for cluster interactions. These interactions are in the form of accurately shifting the expansions of one cluster to the center of another cluster. Subsequently, these expansions are used to determine the velocities of the particles in the second cluster. This has as an effect the minimization of the tree traversals for the individual particles requiring only  $\mathcal{O}(N)$  operations.

The construction and traversing of the tree data structure has been efficiently vectorized so that about 85% of the computational time is spent on the (ultimately unavoidable) pairwise interactions (Eq. (6)) of the vortices within each minimal cluster. Thus the use of the smoothing function  $\eta_\varepsilon$  directly affects the computational cost of the method. The problem may be circumvented by employing careful detailed

tabulations of the smoothing function. For example, the use of tabulated values instead of the calculation of the exponential in the Gaussian smoothing resulted in a fivefold decrease of the computational cost. In its present implementation the velocity evaluation for a million vortices requires 25 CPU seconds on the CRAY-C 90. The velocity evaluations amount to more than 90% of the total computational cost of each simulation. Thus, for a given spatial discretization (with error  $\varepsilon^m$ ) the computational cost ( $\mathcal{C}$ ) for  $N_{\text{steps}}$  time steps, may be expressed in CPU hours as

$$\begin{aligned}\mathcal{C} &\approx c \times 10^{-8} \sum_{i=1}^{N_{\text{steps}}} N(i\delta t) \\ &\approx c \times 10^{-8} \times N_{\text{steps}} \times N^{\text{avg}},\end{aligned}\quad (7)$$

where  $c$  depends on the use of tabulation or direct evaluations of the smoothing function (typically ranging from 0.75 to 4) and  $N^{\text{avg}}$  is an average number of computational elements used throughout the course of the simulations. As the dominant dissipation of the present scheme is attributed to the time discretization, using a second order Adams–Bashforth scheme, the accuracy of the method (roughly speaking) increases proportionally with the square of the computational cost. Practice dictates that this is a conservative estimate. (A version of the code can be obtained from the author.)

## 2. LAGRANGIAN GRID DISTORTION-REMESHING

The advantage of Lagrangian methods over classical Eulerian schemes is the adaptivity of the employed grid (the particles). However, a Lagrangian grid may become highly strained limiting the time to which a purely Lagrangian computation may be taken. Particles may cease to overlap thus violating the convergence criterion of vortex methods dictating that particles must overlap at all times [11, 2].

We are interested then in replacing this (occasionally) strained grid with a new Lagrangian regular grid and simultaneously transport accurately the global flow quantities (such as the total circulation and impulse) from the old grid to the new. This procedure allows us to continuously introduce computational elements when necessary to resolve the increasingly complex vortex structures developing in the flows under consideration.

To restore a regular Lagrangian grid, on the old particles we overlay a cartesian grid (the new particles). The issue is then how to interpolate the old vorticity field ( $\omega$ ) and (distorted) particle locations ( $x$ ) to the new grid (particle) locations ( $\tilde{x}$ ) and obtain a new vorticity field ( $\tilde{\omega}$ ) such that:

$$\tilde{\omega}(\tilde{x}) \approx \omega(x) \quad (8)$$

Alternatively, if  $\tilde{\Gamma}$ ,  $\Gamma$  denote the new and old particle strengths respectively, we are interested in determining an appropriate interpolation kernel  $\Lambda$  so that:

$$\tilde{\Gamma}_i(\tilde{x}_i) \approx \sum_{j=1}^M \Gamma_j(x_j) \Lambda(\tilde{x}_i - x_j). \quad (9)$$

The process is not of the usual interpolation type as it is complicated by the fact that the particles are disordered. The basic analysis of interpolation of this type is given by Schoenberg [27]. He has developed interpolation formulas that attempt to minimize the effect of the grid disorder on the interpolated quantity.

2.1. *Interpolation Kernels*

We may distinguish between two types of interpolation formulae: the collocation type interpolation where  $\tilde{\Gamma}(x_j) = \Gamma(x_j)$ , and the smoothing interpolation, where  $\tilde{\Gamma}(x_j) \neq \Gamma(x_j)$ . If  $h$  is the spacing of the new grid setting  $u = |x|/h$  then interpolation kernels of the first type are:

*Zeroth order interpolation,*

$$\Lambda_0(u) = \begin{cases} 1, & \text{if } 0 \leq u \leq 1/2, \\ 0, & \text{otherwise,} \end{cases} \tag{10}$$

which is the nearest grid point (NGP) interpolation;

*Linear interpolation,*

$$\Lambda_1(u) = \begin{cases} 1 - u, & \text{if } 0 \leq u \leq 1, \\ 0, & \text{otherwise,} \end{cases} \tag{11}$$

which is usually the choice in Cloud in Cell [5] schemes;

*Second-order Interpolation,*

$$\Lambda_2(u) = \begin{cases} 1 - u^2, & \text{if } 0 \leq u < 1/2, \\ (1 - u)(2 - u)/2, & \text{if } 1/2 \leq u < 3/2, \\ 0, & \text{otherwise;} \end{cases} \tag{12}$$

*Everett’s formula of third order,*

$$\Lambda_3(u) = \begin{cases} (1 - u^2)(2 - u)/2, & \text{if } 0 \leq u < 1, \\ (1 - u)(2 - u)(3 - u)/6, & \text{if } 1 \leq u < 2, \\ 0, & \text{otherwise.} \end{cases} \tag{13}$$

The  $\Lambda_M$  ( $M = 0, 1, 2, \dots$ ) kernels may be constructed in a systematic way so as to ensure conservation of the first  $M$  moments of the vorticity field ( $M = 0$ , implies the conservation of circulation). This may be easily exemplified by considering the following derivation of the interpolation formulas. We may consider for simplicity the one dimensional case, of a particle of unit strength ( $\Gamma = 1$ ), having core radius,  $\epsilon$ , located at  $(x_0)$  and inducing a vorticity field  $\omega(x) = \eta((x - x_0)/\epsilon)$ . We are interested in replacing this particle by  $M$  particles at equally spaced locations  $(\tilde{x}_m)$ , having strength  $(\tilde{\Gamma}_m)$  so as to obtain an “equivalent” vorticity distribution. The vorticity at a location  $x$  is given as



$$\begin{aligned} \omega(x) &= \eta((x - x_0)/\varepsilon) \\ &\approx \sum_{m=1}^M \tilde{\Gamma}_m \eta((x - \tilde{x}_m)/\varepsilon) = \tilde{\omega}(x). \end{aligned} \tag{14}$$

One cannot expect an ‘‘exact’’ solution to the above equation for the unknown values  $\tilde{\Gamma}_m$ , for all locations  $x$ . However, one may try to:

- conserve as many moments ( $T_a$ ) of the vorticity ( $T_a = \int \omega(x)x^a dx$ ), as possible ( $a = 0, 1, 2, \dots$ ) and
- minimize the error at distances larger than the mesh size.

Taking the Fourier transform of the previous equation we have

$$\begin{aligned} \mathcal{F}\mathcal{F}\{\omega(x)\} &= e^{-ikx_0} \mathcal{F}\mathcal{F}\left\{\eta\left(\frac{x}{\varepsilon}\right)\right\} \\ &\approx \mathcal{F}\mathcal{F}\left\{\eta\left(\frac{x}{\varepsilon}\right)\right\} \sum_{m=1}^M \tilde{\Gamma}_m e^{-ik\tilde{x}_m}, \end{aligned} \tag{15}$$

or equivalently, we ask that the new particles have to satisfy the equation:

$$\sum_{m=1}^M \tilde{\Gamma}_m e^{ik(x_0 - \tilde{x}_m)} \approx 1. \tag{16}$$

Defining  $\Delta_{0m} = x_0 - \tilde{x}_m$  and expanding the left-hand side for small values of  $\tau_{0m} = k \Delta_{0m}$  (as the smoothing kernels decreases exponentially with  $k$ ) we obtain

$$\sum_{m=1}^M \tilde{\Gamma}_m \left( 1 + i\tau_{0m} - \frac{1}{2}\tau_{0m}^2 + \mathcal{O}(\tau_{0m}^3) \right) \approx 1. \tag{17}$$

Note that this equation is independent of the shape function  $\eta$  and the core radius  $\varepsilon$ . Having  $M$  as the free parameter in the above equation we see that we can approximate the vorticity field to the extent possible by requesting that  $M$  terms are satisfied in the above equation. We may systematically construct the interpolation kernels that obey the above requirements by employing more and more mesh-points. However, computational cost becomes a factor and one usually avoids using  $M > 5$ . For  $M = 1$  we can conserve only the circulation by assigning the circulation of each particle to its nearest mesh point (the NGP scheme). Solving the above sets of equations for  $M = 2, 3, 4$  we obtain respectively the interpolating kernels  $\Lambda_1, \Lambda_2, \Lambda_3$ , which conserve the first, second, and third moment of the vorticity field, by employing  $2^d, 3^d, 4^d$  mesh points (with  $d$  the dimension of the problem). With each interpolation scheme we may associate a hyperviscous type of dissipation introduced by the remeshing procedure, as they conserve a finite number of vorticity moments. Negative vorticity may be generated by the outer layers of remeshed particles, as the higher order remeshing functions (such as  $\Lambda_2$ ) generate negative particle strengths to attain their accuracy. This may impose some limitations on

the use of these formulas when interpolating quantities (for example, a density field) for which negative values are unphysical. However, this is not the case for the vorticity field. The vorticity field is computed as a linear superposition of the vorticity field (Eq. (5)) introduced by all the particles so that the effect of negative particle strengths does not pose such difficulties.

The interpolation schemes act as low pass filters, removing all the high-order harmonics that arise from the irregularity of the grid. Simultaneously they determine the smaller scales of the vorticity field we expect to resolve in our simulations. However, they do not have continuous derivatives and second and higher order kernels are not even continuous. This implies that when interpolating quantities having large fluctuations for small particle separation they might introduce large interpolation errors from small errors in the actual particle locations. The second type of interpolation attempts to minimize such effects. Schoenberg [27] has introduced a set of such interpolation kernels the *central B-splines* ( $M_n$ ). The formulae for the first two members of the family coincide with the  $\Lambda$  kernels, the  $M_3$  function is the first one to have a continuous first derivative and is usually referred to as the TSC (triangular shaped cloud) function. For reference we give here the  $M_4$  kernels.

$$M_4(u) = \begin{cases} 1/6(2-u)^3 - 4/6(1-u)^3 & \text{if } 0 \leq u \leq 1, \\ 1/6(2-u)^3 & \text{if } 1 \leq u \leq 2, \\ 0 & \text{otherwise.} \end{cases} \quad (18)$$

The B-splines act as better low pass filters (their Fourier transform is given by  $(\sin \alpha/\alpha)^M$ , with  $\alpha = \pi kh$ ), but they conserve only the circulation and the linear momentum of the vorticity field. B-Splines have an accuracy of  $\mathcal{O}(h^2)$  so they can interpolate exactly only linear functions. Monaghan [23] has presented a systematic way of increasing the accuracy of interpolating functions while maintaining their smoothness properties. For the B-splines, however, such an improvement is possible only for  $M \geq 3$ . We present here the improved interpolating formula that corresponds to the  $M_4$  listed above:

$$M'_4(u) = \begin{cases} 1 - \frac{5u^2}{2} + \frac{3u^3}{2}, & \text{if } 0 \leq u \leq 1, \\ \frac{1}{2}(2-u)^2(1-u), & \text{if } 1 \leq u < 2, \\ 0, & \text{otherwise.} \end{cases} \quad (19)$$

Note that this kernel gives now an ordinary interpolation formula which reproduces polynomials of order 2. In general B-Splines are able to accurately interpolate smooth functions but they fail to represent functions with very steep gradients. Higher order harmonics introduced by the particle disorder are dampened at the expense of additional numerical dissipation. An extensive survey of the Fourier space analysis of these schemes may be found in the book of Hockney and Eastwood [12].

The computational cost of the remeshing procedure is minimal as the strengths of the new remeshed particles are directly determined by Eq. (8). The key issue is the identification of the particles on the remeshed grid affected by each old particle. An efficient indexing of the new particle locations allows for this identification using simple integer number calculations, so that the cost of the remeshing step scales linearly with the number of old particles. A remeshing step required about 2 CPU seconds on the CRAY C-90 for the remeshing of 100,000 particles onto a new set of 100,000 particles, using the  $\Lambda_2$  kernel. As the remeshing occurs every 7 to 10 time steps it corresponds only to a small fraction (less than 1%) of the overall computational cost of the algorithm.

### 3. INITIALIZATION—DIAGNOSTICS

In this study we consider the evolution of compact elliptical (2:1) vortices. Two radially symmetric profiles were considered. They may be described as ( $r = \sqrt{x^2 + y^2}$ ),

$$\omega^I(r) = \Lambda \begin{cases} 1 - f_q(r/R_0), & \text{if } r \leq R_0, \\ 0, & \text{otherwise,} \end{cases} \tag{20a}$$

where  $f_q(z) = \exp(-q/z) \exp(1/(z - 1))$ . This vorticity profile was suggested by MMZ as a good compromise between profiles that can be simulated using pseudospectral and contour dynamics methodologies. Following MMZ the values  $q = 2.56085$  and  $\Lambda = 20$  and  $R_0 = 0.8$  were selected. The second profile that was selected for the present simulations corresponds to the eight-level piecewise continuous vorticity profile examined by Dritschel [7],

$$\omega^{II}(r) = \Lambda \begin{cases} 1 - (r/R_0)^4, & \text{if } r \leq R_0, \\ 0, & \text{otherwise.} \end{cases} \tag{20b}$$

using the same values for  $\Lambda$  and  $R_0$  (Fig. 1).

In this work a series of parametric studies is conducted to assess the numerical dissipation of the method. In all these studies the profile  $\omega^I$  was considered. The results of these studies suggested suitable numerical parameters for the simulation of the evolution of  $\omega^{II}$ .

To *initialize* the computation a regular cartesian grid is laid over the support of the elliptical vorticity distribution and the centers of the grid cells ( $x_n, y_n$ ) consist the initial particle locations. The initial particle strengths ( $\Gamma_n$ ) are determined by solving the set of equations

$$\sum_n A_{mn} \Gamma_n = \omega(x_m, y_m), \quad m = 1, \dots, N \tag{21}$$

where  $A_{mn} = \eta_\varepsilon(x_m - x_n, y_m - y_n)$ . This system of equations is solved iteratively as its size prohibits direct inversion. It was found that the system is solved most effectively using the method of *SOR*, with a coefficient in the range of 0.3 to 0.4 (underrelaxation).

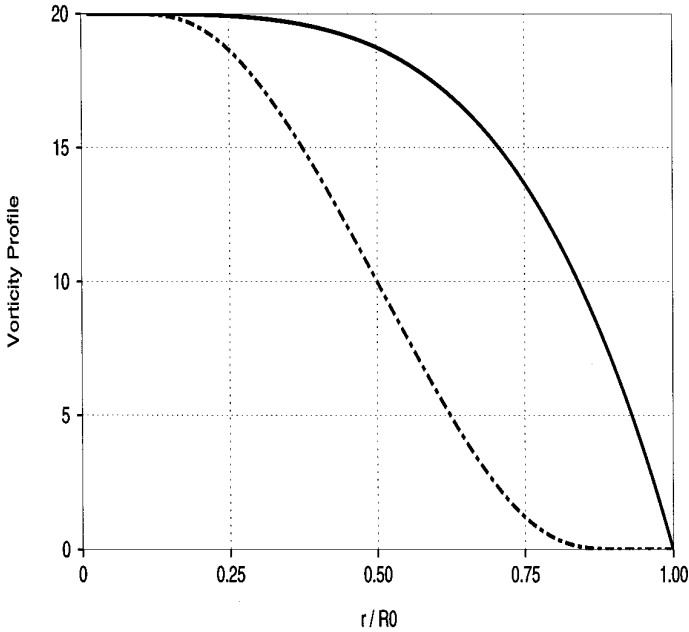


FIG. 1. Initial vorticity profiles:  $\omega^I$  (dot-dash) and  $\omega^{II}$  (solid line).

### 3.1. Vorticity Moments

For inviscid flows vorticity moments are conserved and, hence, their variation with time in computations help us identify the dissipation of the numerical scheme. Moreover, vorticity moments help us interpret the evolution of the global characteristics of the flow.

Following Dritschel [7] we define the parameter  $J_{mn}$  as

$$J_{mn} = \iint \omega(x, y) x^m y^n dx dy. \quad (22)$$

In vortex methods the calculation of these quantities is facilitated by the analytical expression for the vorticity field (Eq. (5)). For example, when using Gaussians as smoothing functions the angular impulse of the vorticity field may be calculated explicitly as

$$J_g = \sum_{n=1}^N \Gamma_n (x_n^2 + y_n^2 + \varepsilon^2).$$

Vorticity moments cannot be easily evaluated in closed form for all smoothing functions. In order to maintain a uniformity in our approach in evaluating these expressions we use a simple quadrature rule. The values of the vorticity are computed on equispaced rectangular grid locations  $(x_k, y_k)$ , using the definition of the vorticity (Eq. (5)) as

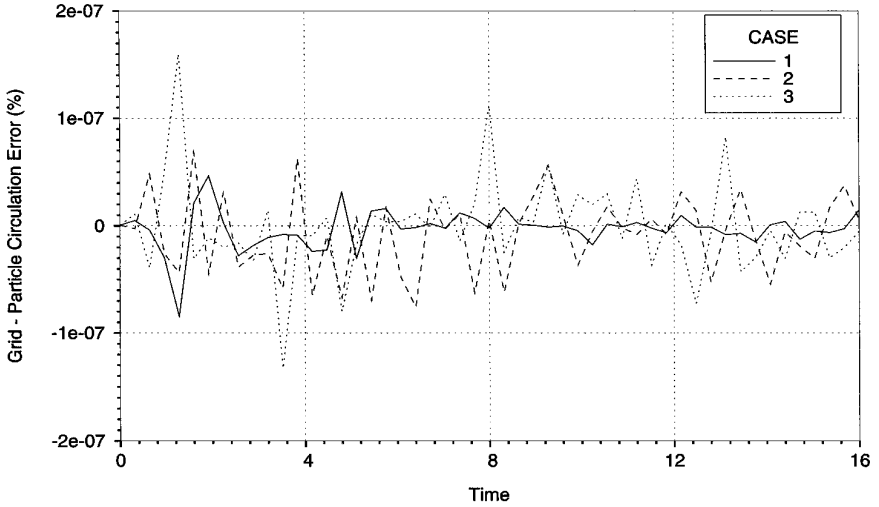


FIG. 2. Error between the computation of the total circulation as computed using the particle strength and the grid information for Cases 1, 2, 3.

$$\omega(x_k, y_k) = \sum_{n=1}^N \Gamma_n \eta_n(x_n - x_k, y_n - y_k). \tag{23}$$

These grid values are then used to compute the integrals associated with the vorticity moments. For example, the angular impulse is computed as

$$J = J_{02} + J_{20} = \sum_{k=1}^{M \text{ grid}} \omega(x_k, y_k)(x_k^2 + y_k^2) \delta x_k \delta y_k, \tag{24}$$

where  $\delta x_k, \delta y_k$  are the local grid spacings in the  $x$  and  $y$  directions. During the postprocessing of the present simulations the following (nominally conserved) vorticity moments have been computed: circulation ( $J_{00}$ ), linear impulse ( $J_{10}, J_{01}, J_{11}$ ), and angular impulse ( $J_{02}, J_{20}$ ). The accuracy of the approach of computing the integrals using the grid values versus the respective quantities that would have been computed from the particle values is shown in Fig. 2 for the computation of circulation. There is an excellent agreement of the two approaches to compute the integral quantities. In the rest of this work the integrals are computed using the grid based values of the vorticity.

In order to quantify the numerical dissipation of the present simulations we considered the effective viscosity defined as

$$\nu^{\text{eff}}(t) = \frac{J(t) - J(0)}{4\Gamma(t)t}$$

which is nondimensionalized using the circulation of the vorticity field, so that a time varying, effective dissipative ‘‘Reynolds’’ number may be defined as

$$\text{Re}^{\text{eff}}(t) = \frac{\Gamma(t)}{\nu^{\text{eff}}(t)}. \quad (25)$$

The phenomenon of axisymmetrization can be quantified by considering the effective aspect ratio of the vortical structures defined as [7]

$$\lambda_{\text{eff}}^2 = \frac{J + R}{J - R}, \quad (26)$$

where  $R^2 = D^2 + 4J_{11}^2$  and  $D = J_{20} - J_{02}$  and  $J = J_{20} + J_{02}$ .

### 3.2. The Energy Spectrum

The energy spectrum of a vorticity field may be computed as [19]

$$\mathcal{E} = \int \frac{|\hat{\mathbf{u}}|^2}{2} d\mathbf{k} \quad (27)$$

and with  $d\mathbf{k} = k dk d\theta$  we have

$$\mathcal{E} = \int E(k) dk \quad (28)$$

with  $E(k) = \int (|\hat{\mathbf{u}}|^2/2)k d\theta$ . From the definition of vorticity we get  $\hat{\mathbf{u}}(k) = i\mathbf{k} \times \hat{\boldsymbol{\omega}}/k^2$  so that  $|\hat{\mathbf{u}}|^2 = |\hat{\boldsymbol{\omega}}|^2/k^2$ . The vorticity field is defined as the superposition of the vorticity fields in Eq. (5) so that

$$\hat{\boldsymbol{\omega}}(k) = \int \boldsymbol{\omega}(\mathbf{x})e^{i\mathbf{k}\cdot\mathbf{x}} d\mathbf{x} = \hat{\eta}_\varepsilon(k) \sum_{n=1}^N \Gamma_n(t)e^{i\mathbf{k}\cdot\mathbf{x}_n}, \quad (29)$$

where  $\hat{\eta}_\varepsilon(k)$  signifies the Fourier transform of the cutoff function  $\eta_\varepsilon(x)$ . Finally, we would have that

$$|\hat{\boldsymbol{\omega}}|^2 = \hat{\eta}_\varepsilon^2 \sum_m \sum_n \Gamma_m \Gamma_n e^{i\mathbf{k}\cdot(\mathbf{x}_m - \mathbf{x}_n)}. \quad (30)$$

Using now the result that  $\mathbf{k}\cdot(\mathbf{x}_m - \mathbf{x}_n) = k|\mathbf{x}_m - \mathbf{x}_n|\cos\theta$  and that

$$\int_0^{2\pi} e^{ik|\mathbf{x}_m - \mathbf{x}_n|\cos\theta} d\theta = 2\pi J_0(k|\mathbf{x}_m - \mathbf{x}_n|), \quad (31)$$

where  $J_0$  is the zeroth-order Bessel function, we obtain

$$E(k) = \pi \frac{\hat{\eta}_\varepsilon(k)^2}{k} \sum_m \sum_n \Gamma_m \Gamma_n J_0(k|\mathbf{x}_m - \mathbf{x}_n|). \quad (32)$$

Note that the Fourier transform of smoothing functions is not always readily available. To circumvent this difficulty the vorticity field is computed at the grid locations using the vorticity equation and subsequently this pointwise information (hence,  $\hat{\eta}_\varepsilon(k) = 1$ ) is used to compute the energy spectrum of the vorticity field (Fig. 9). Equation (32) facilitates the understanding of the energy spectrum in terms

**TABLE I**  
**Computational Parameters of the Convergence Study**

Case	$\delta t (\times 10^3)$	$\varepsilon^2 (\times 10^3)$	Cutoff( $\eta_\varepsilon$ )	Nrem
1	16	1.00	Gaussian	5
2	8	1.00	Gaussian	9
3	4	1.00	Gaussian	17
4	4	0.60	Gaussian	17
5	4	0.60	Gaussian	9
6	8	5.00	Super-Gauss.	9
7	8	1.00	Super-Gauss.	9
8	4	1.00	Super-Gauss.	9
9	4	0.50	Super-Gauss.	7
10	1	0.05	Gaussian	9

of the shape of the vortical structures. For example, for a compact circular vortex with radius  $R$  and total circulation  $\Gamma$  the energy spectrum may be expressed as:  $E(k) = \Gamma^2 J_1^2(kR) / (\pi R^2 k^3)$ .

#### 4. VALIDATION STUDIES

In order to assess the effects of the various numerical parameters on the results of the simulations and to quantify numerical dissipation of the present method a systematic convergence study was conducted.

The evolution of the  $\omega^l$  profile was examined as we varied the remeshing frequency (Nrem), the time step ( $\delta t$ ), the core size ( $\varepsilon$ ), and the smoothing function ( $\eta_\varepsilon$ ) of the particles. The parameters used in each case are shown in Table I.

In case 10 the time step was kept to 1E-03 for  $T = 0$  to 8 and was increased to 2E-03 for  $T = 8$  to 12 and to 4E-03 for  $T = 12$  to 24. The number of computation (Fig. 3) elements increases with the progressive evolution of the vorticity field as the grid automatically adapts to resolve the complex structures of the flow.

##### 4.1. The Effect of Time Step ( $\delta t$ )

In all our simulations a second-order Adams–Bashforth scheme (with expected error proportional to  $(\delta t)^2$ ) has been used to advect the particle locations thus requiring only one velocity evaluation per time step. The effect of the time step may be assessed by observing the numerical dissipation of the scheme as measured by the effective ‘‘Reynolds’’ number ( $R_e^{\text{eff}}$ ) (Eq. (25)). As depicted in Fig. 5 for cases 1 through 10, there is a remarkable collapse in the effective dissipation data, as scaled by the time step used in each case.

Moreover, after an initial transient coinciding with the onset of the filamentation process, the  $R_e^{\text{eff}}$  remains practically constant, implying a second-order diffusive character for the numerical dissipation. This dependence of the numerical dissipation on the time step may be further evaluated by observing that as the time step in case 10 was doubled, a respective gradual increase was observed in the numerical

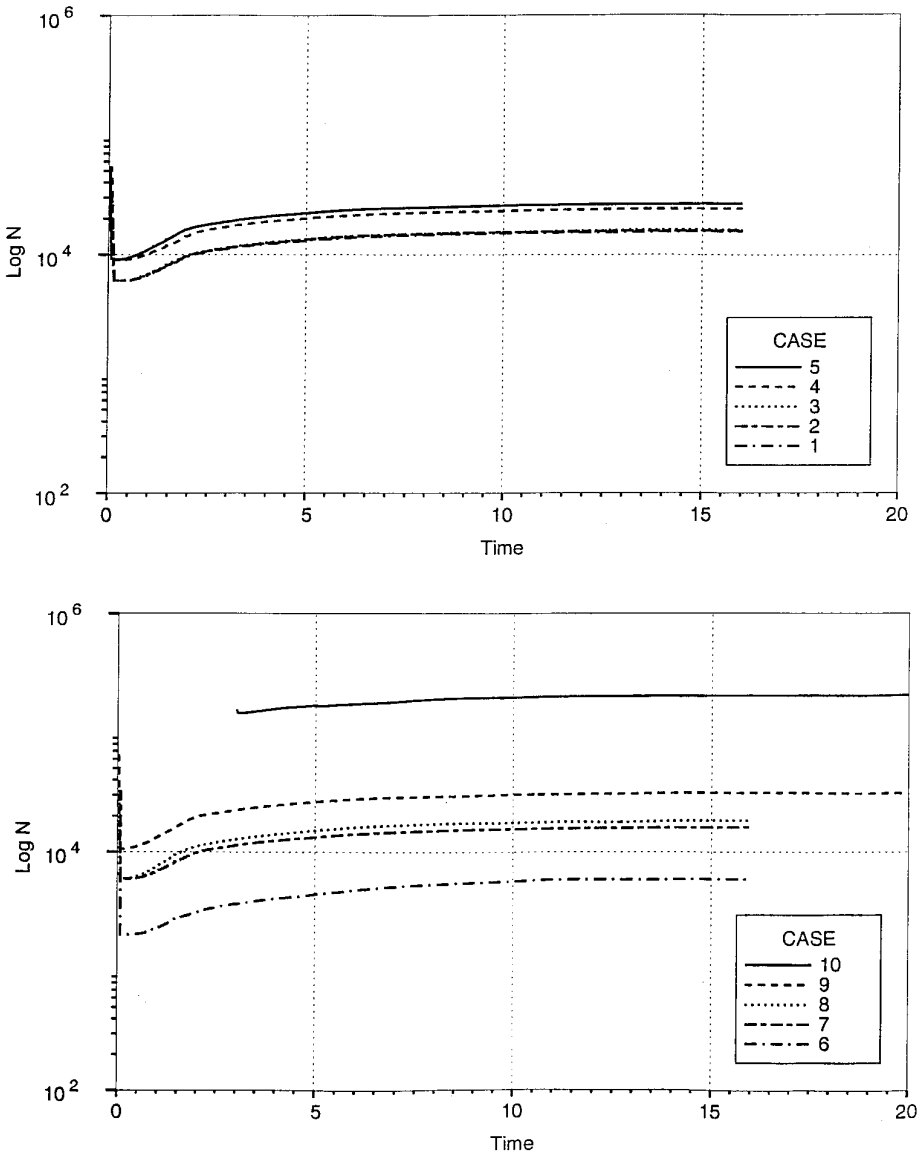


FIG. 3. Logarithmic variation of the number of computational elements ( $N$ ) with time.

dissipation. The dissipation in the third stage of the simulation in case 10 ( $\delta t = 4 \times 10^{-3}$ ) asymptotes to the dissipation observed in case 9, which employs the same time step. The second-order diffusive character of the numerical dissipation is further exemplified by the remarkable agreement (Fig. 5) in the  $R^{\text{eff}}$  in the evolution of  $\omega^I$  (as simulated in case 5) and  $\omega^{II}$  (simulated with the same numerical parameters as in case 5). We may conclude that the dominant dissipative error of the present scheme is introduced by the time discretization of Eq. (6) and has a diffusive character (proportional to  $\nu^{\text{eff}} \nabla^2 \omega$ ). However, the  $\nu^{\text{eff}}$  can be consistently reduced by accordingly reducing the time step.



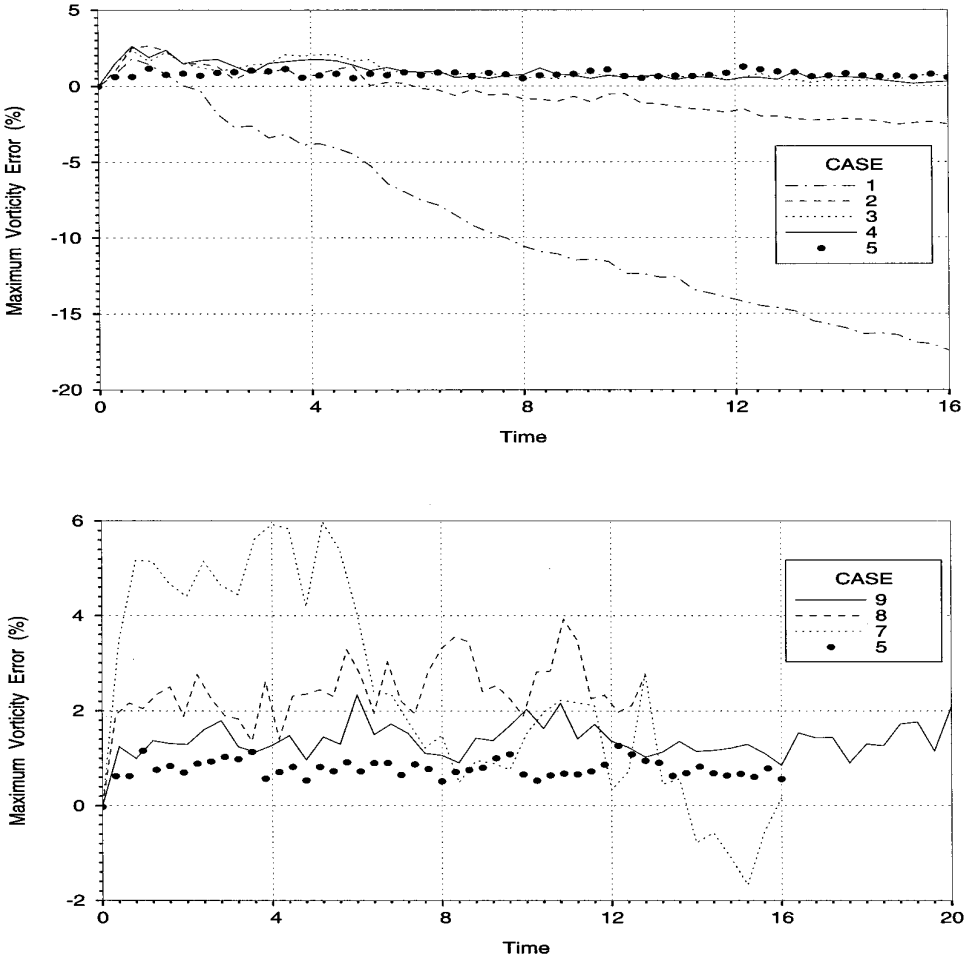
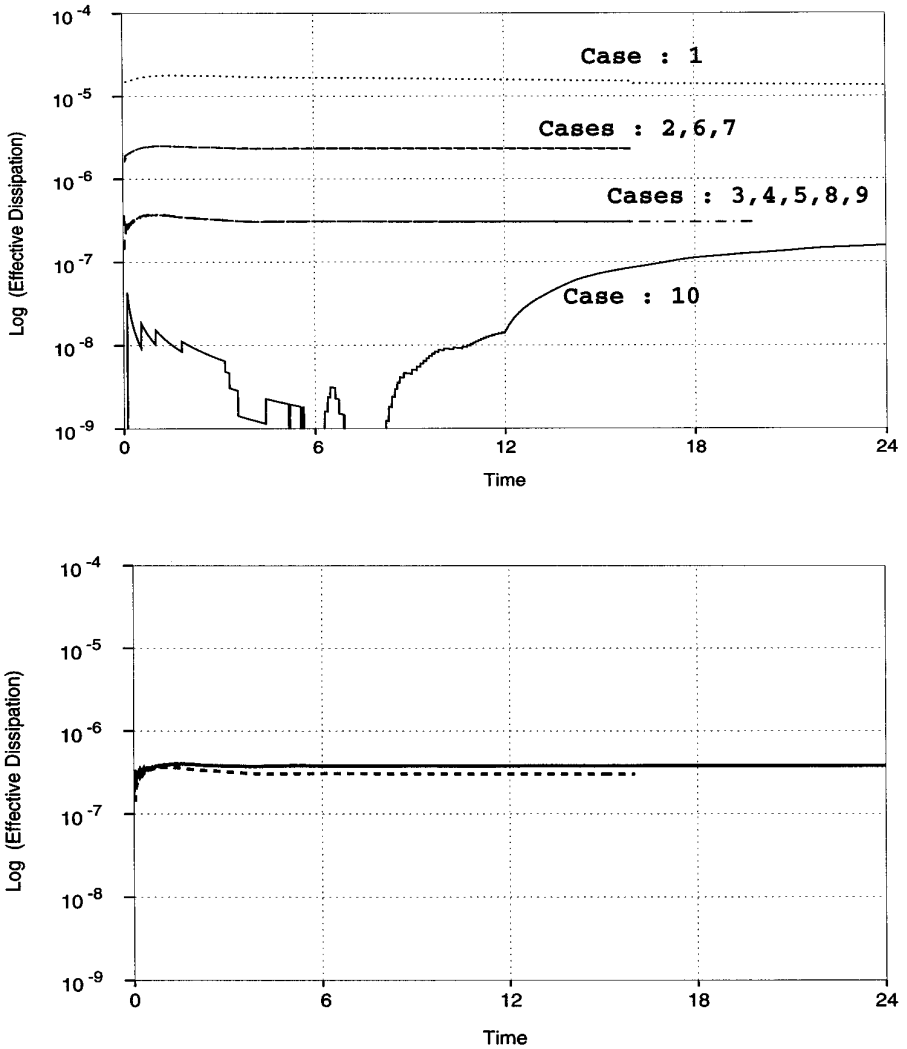


FIG. 4. Parametric study of the relative error in the conservation of maximum vorticity.

Errors related to the time-stepping may be observed also in the nonconservation of the maximum vorticity. However, as the remeshing frequency was kept constant, these may be mainly attributed to the increasing time interval between remeshing steps. On the other hand, the enstrophy decrease (Fig. 6) appears more strongly dependent on the spatial approximation of the vorticity field. The effect of the time step is far less significant than the respective error introduced by the shape (smoothing error) and core size (quadrature error) of the selected core function.

4.2. The Effect of Remeshing

In order to assess the effect of remeshing we may compare the results of cases 4 and 5 for which the rest of the parameters were kept constant. The error in the conservation of maximum vorticity is reduced by increasing the remeshing frequency. The error is more significant at the earlier stages of the evolution of the



**FIG. 5.** Effective nondimensional viscous dissipation  $1/R_c^{\text{eff}}$ : Parametric study for (a)  $\omega^I$  and (b) comparison of the dissipation for the evolution of  $\omega^I$  (dashed line) and  $\omega^{II}$  using the parameters of Case 5.

elliptical vortex as the particles in the central core undergo significant stretching thus not maintaining overlap. It appears that a smaller remeshing interval would have been necessary at the earlier stages of the evolution of the ellipse, whereas a larger remeshing interval would have been adequate at the later stage of the evolution. Criteria for establishing an automatic, variable remeshing frequency have not been adopted yet. The results of the present simulations may offer some input for further research in this direction.

As discussed earlier remeshing using higher order remeshing functions, introduces a hyperviscous type of dissipation in these simulations. This effect may be assessed by comparing the numerical dissipation in the evolution of  $\omega^I$  (as computed using the parameters in case 5) and  $\omega^{II}$ . As it is discussed in Section 5,  $\omega^{II}$  was evolved

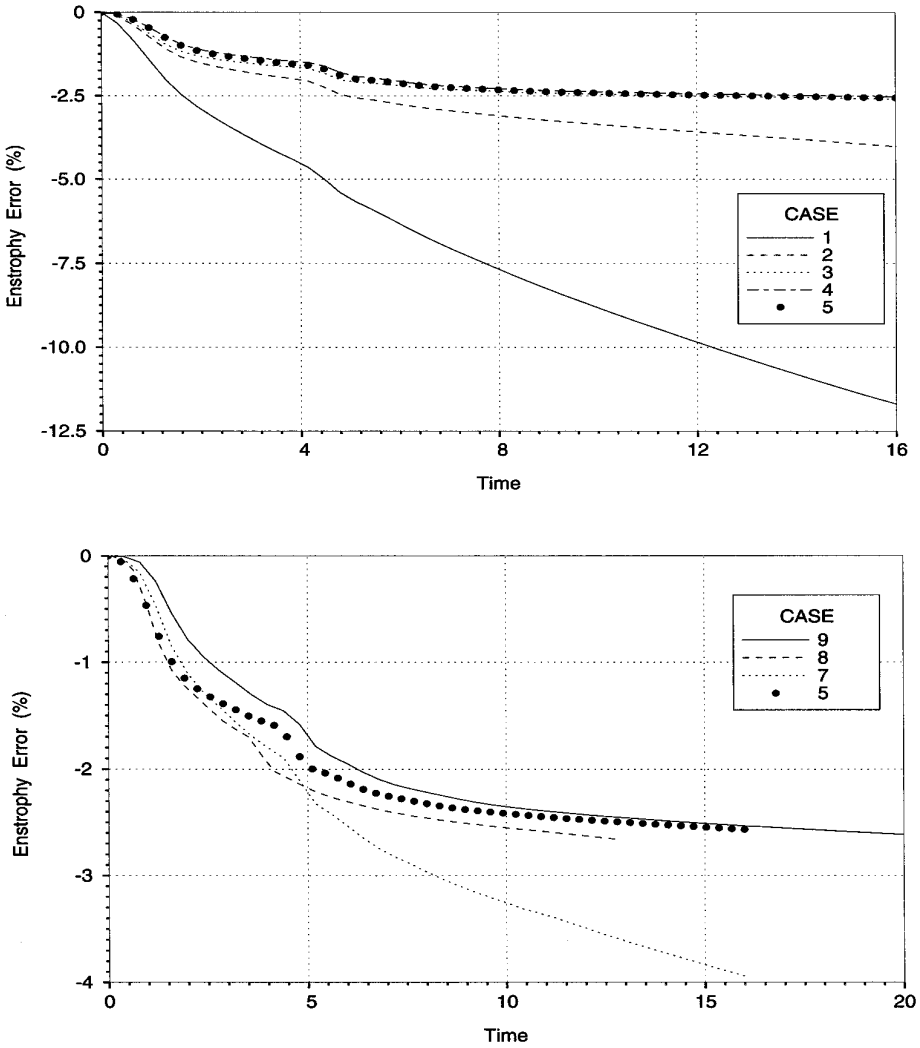


FIG. 6. Parametric study for the conservation of enstrophy for the evolution of  $\omega^I$ .

using the parameters described in case 5 with the remeshing function  $M_4^I$ . The  $\Lambda_2$  scheme was used in the remeshing of  $\omega^I$ . In both cases negative vorticity in the periphery of the vortical structures did not exceed the 0.05% threshold. The effective dissipation of the two schemes as plotted in Fig. 5 is indistinguishable. As the interpolation associated with remeshing is not performed at each time step (as is, for example, the case in Cloud in Cell calculations) the hyperviscous effects do not dominate the physics of the simulations. Numerical dissipation is dominated by the time discretization.

#### 4.3. The Effect of Core Size ( $\epsilon$ )

The effect of the core size is associated with the error of the approximation of the singular operators by smooth operators. For the case of a Gaussian core this

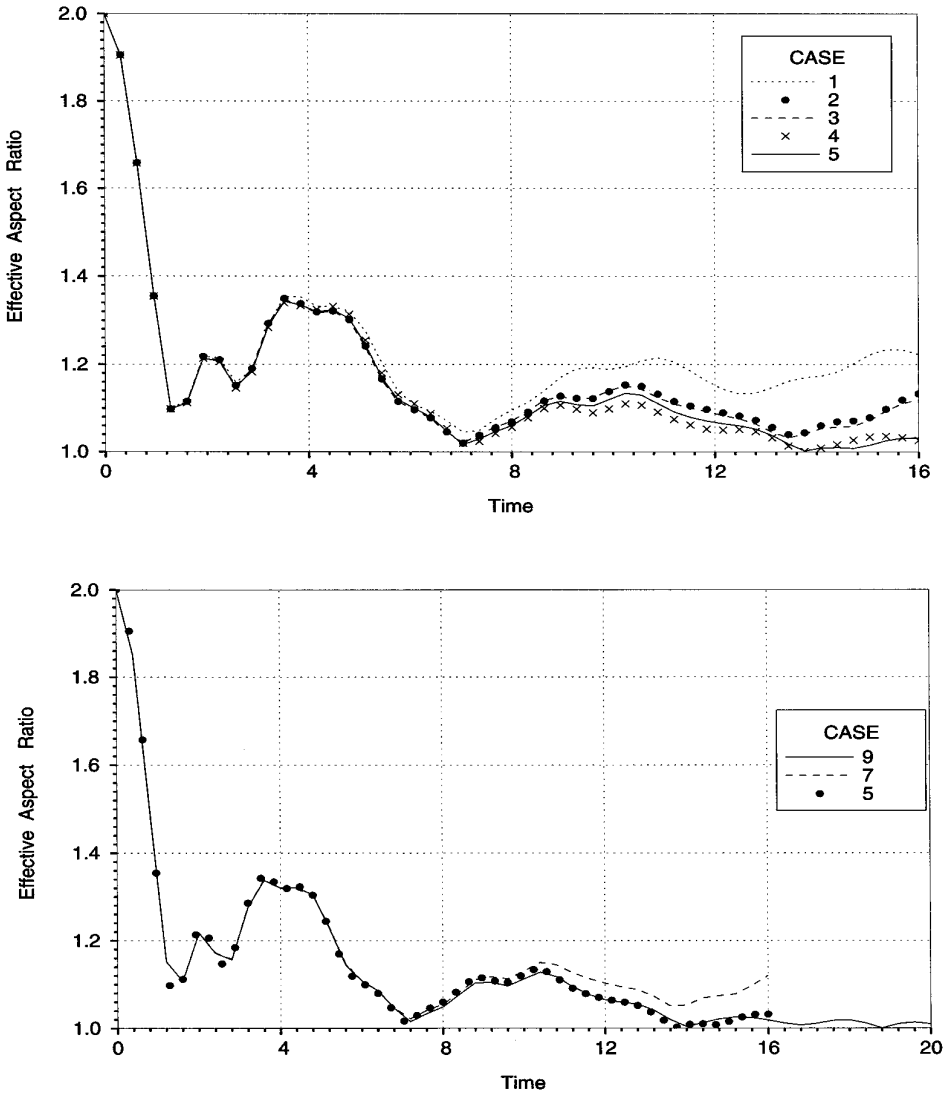


FIG. 7. Parametric study on the evolution of the effective aspect ratio ( $\lambda_{\text{eff}}$ ) of the vorticity field  $\omega^l$ .

effect may be assessed by comparing the results of cases 3 and 4. A discrepancy is observed in the computed aspect ratio (Fig. 7). The  $\lambda_{\text{eff}}$  computed in cases with smaller core radius, converge towards the value obtained by higher resolution simulations, especially at the later stages of the evolution of the vorticity field. The effect of core size when implementing super-Gaussians may be assessed by examining the enstrophy decrease in cases 8 and 9 (Fig. 6). The effects of core size reduction are more pronounced in the super-Gaussian case as the theory predicts (since there is a higher power exponent associated with the error of the super-Gaussian).

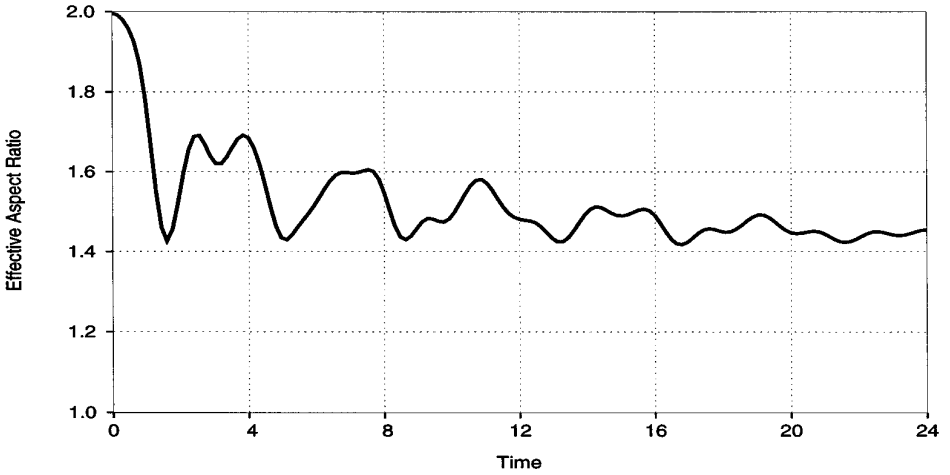


FIG. 8. Evolution of the effective aspect ratio ( $\lambda_{\text{eff}}$ ) of the vorticity field  $\omega^{\text{II}}$ .

#### 4.4. The Effect of Core Shape ( $\eta_c$ )

The effect of the core shape may be evaluated by examining the diagnostics from cases 2 and 7, as well as the results of cases 3 and 8. The most significant discrepancy is observed in the plots for the maximum vorticity (Fig. 4) and for the effective dissipation (Fig. 5). The results of the simulations suggest that when using a higher order smoothing function the details of the particle overlap are magnified thus affecting the global diagnostics of the flow. Hence, one may observe a significantly higher error in tracking of the maximum vorticity as compared to that by the simple Gaussian kernel. The error seems to diminish at the later stages of the ellipse evolution when a more “quiet” flow is established, becoming comparable and less significant than the error in respective simulations using Gaussian kernels.

## 5. RESULTS

In this section we present the results of the extended time (about  $52T_p$ , where  $T_p = 4\pi/\omega_{\text{max}}$ ) simulations of the inviscid evolution of the two elliptical vortices with initial profiles defined by  $\omega^{\text{I}}$  and  $\omega^{\text{II}}$  (Fig. 1). The results presented for the evolution of  $\omega^{\text{I}}$  are the ones obtained using the numerical parameters described in case 10 (with computational cost  $\ell = 5$  CPU hours). The parameters described in case 5 were used in the simulation of the evolution of  $\omega^{\text{II}}$  (with computational cost  $\ell = 0.30$  CPU hours). The  $\Lambda_2$  and  $M_4$  remeshing functions were employed in the remeshing of the  $\omega^{\text{I}}$  and  $\omega^{\text{II}}$  fields, respectively. The circulation and linear impulse were conserved to roundoff error throughout the simulations. The  $R^{\text{eff}}$  for  $\omega^{\text{I}}$  was in the order of  $10^8$  in the first part of the simulation and decreased to  $10^7$  with the increase of the time step at the later stages. For  $\omega^{\text{II}}$  the  $R^{\text{eff}}$  was maintained around  $2 \times 10^6$ . The vorticity maximum was conserved to within 0.25% and the enstrophy decreased was below 2% at the end of the simulation. Negative vorticity was gener-

ated around the periphery of the main vortex core but it never exceeded 0.05% of the maximum vorticity for both cases.

Hyperviscous pseudo-spectral simulations have reported errors in the conservation of the maximum vorticity ranging from 5 (MMZ) to 30%, while enstrophy was decreased from 10 to 30% depending on the resolution of the simulation [29]. Moreover, spurious negative vorticity (at about 5% MMZ [13]) has been observed to be generated in the periphery of positive vorticity regions. Contour surgery simulations do not usually report diagnostics regarding the conserved moments of the vorticity field. Yao *et al.* [29] report a 2.5% enstrophy decrease in a CS calculation.

Dissipation of similar magnitudes has also been observed in the respective experimental studies. Fine *et al.* [8] report experimental investigations where the circulation, linear and angular impulse of the vorticity field are conserved to within 10%, but rather large discrepancies (up to 40%) are observed in diagnostics such as the maximum vorticity and the enstrophy.

### 5.1. Evolution of the Vorticity Field $\omega^l$ —Axisymmetrization

We may distinguish four stages in the evolution of the elliptical vortex with the initial profile described by  $\omega^l$ , related to the variation of the effective aspect ratio ( $\lambda_{\text{eff}}$ ) with time (Fig. 7).

In the first stage ( $T = 0$  to  $T \approx 1.5$ ) a significant decrease is observed in the eccentricity of the ellipse as it gets reduced by about 90% due to the different rotational speeds of the outer and inner layers of the vorticity distribution.

In Fig. 10 we may observe two strong vortical arms being extracted from the main structure and the link of the main core with the extracted vorticity is progressively reduced. In Fig. 11 this phenomenon is exhibited as relatively high amplitude, low frequency waves on the vorticity profile. At the earlier stages of this process the vorticity profile remains monotonically decreasing. At  $T = 1.0$  we may observe a non monotonic vorticity profile along the  $x = 0$  locations. Such a nonmonotonic vorticity profile is susceptible to a Kelvin–Helmholtz-type instability [25]. At time  $T = 1.5$  such an instability may indeed be observed (Figs. 10 and 11) as azimuthal vortical waves on the surface of the vortex core. Simultaneously on the vorticity profile one may clearly observe the development of sharp vorticity gradients inducing further stripping of vorticity from the main core.

At the start of the second stage ( $T \approx 1.5$  to  $T \approx 7$ ) the azimuthal vortical waves get wrapped around the main vortex core resulting in a decrease of their amplitude. The influence of the vortex core inhibits the rollup of these vortical filaments. The corresponding thinning of the external filaments has as a result a new moderate increase in the ellipticity of the vorticity field. This ellipticity reaches a new local maximum (at  $T \approx 4$ ) when parts of the filaments get reattached along the sides parallel to the major axis of the vortex. Subsequently a new reduction of the ellipticity is observed as the filament reattachment induces a new relatively high amplitude perturbation, as it disturbs the monotonicity of the vorticity profile and triggering further filamentation of the periphery of the vortex core. Further stripping of the vortex core and interaction with the attached filamentary structures leads to a thickening of the core–filament link reinstalling a venue for weak vorticity to

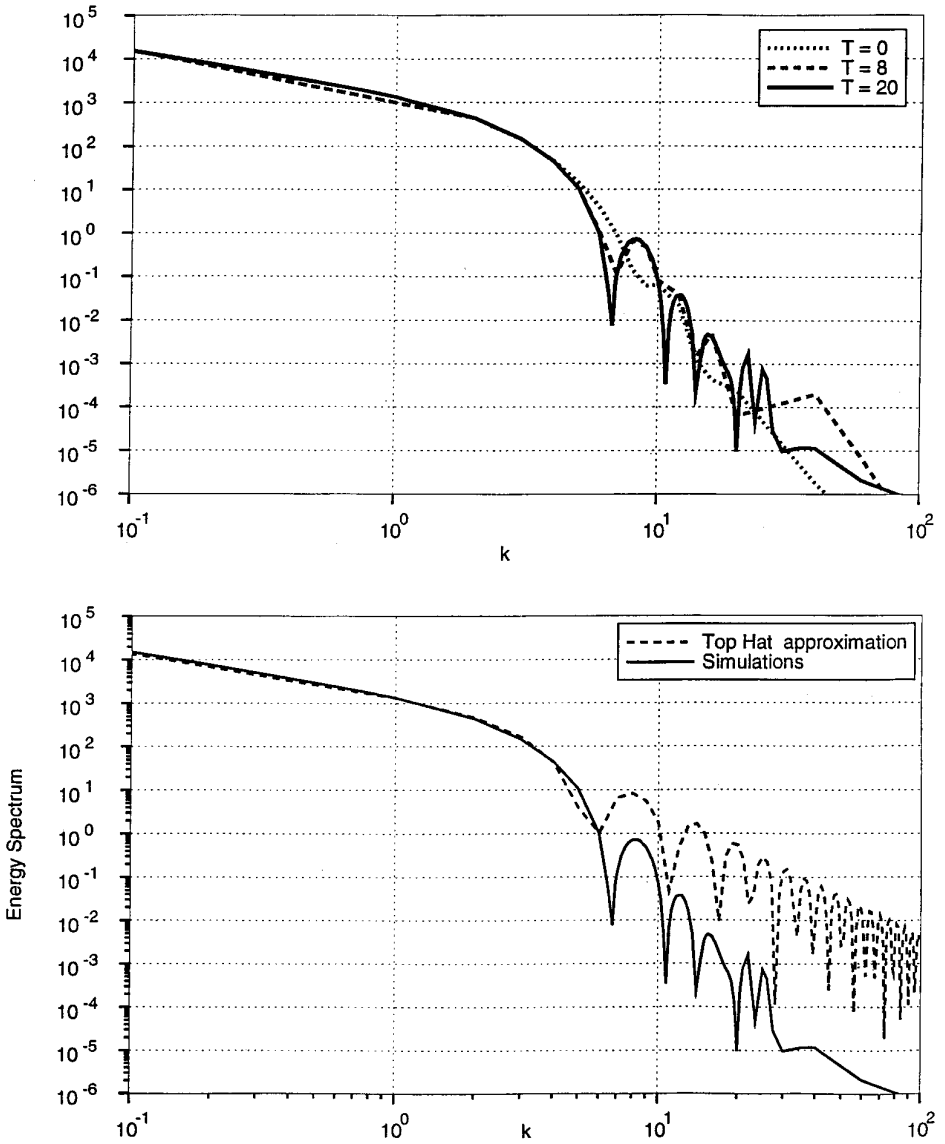


**FIG. 9.** (a) Energy spectrum for the different stages of the evolution of the vorticity field  $\omega^i$ . (b) Comparison of the energy spectrum of the vorticity field at  $T = 24$ , with the energy spectrum of a top-hat profile vortex carrying circulation comparable to that of the vortex core.

propagate away from the core resulting in axisymmetrization of the vortical structure at  $T \approx 7$ .

A similar evolution has been observed in the respective simulations of MMZ. They conclude their simulation at  $T = 8$  claiming that the vorticity field has axisymmetrized and that no further significant evolution of the elliptical vortex is expected. The vorticity contours and the vorticity profiles provided at  $T = 8$  by MMZ and the results of the present simulations show several discrepancies (Figs. 14 and 15). The vorticity profile presented in MMZ shows a smoother profile corresponding

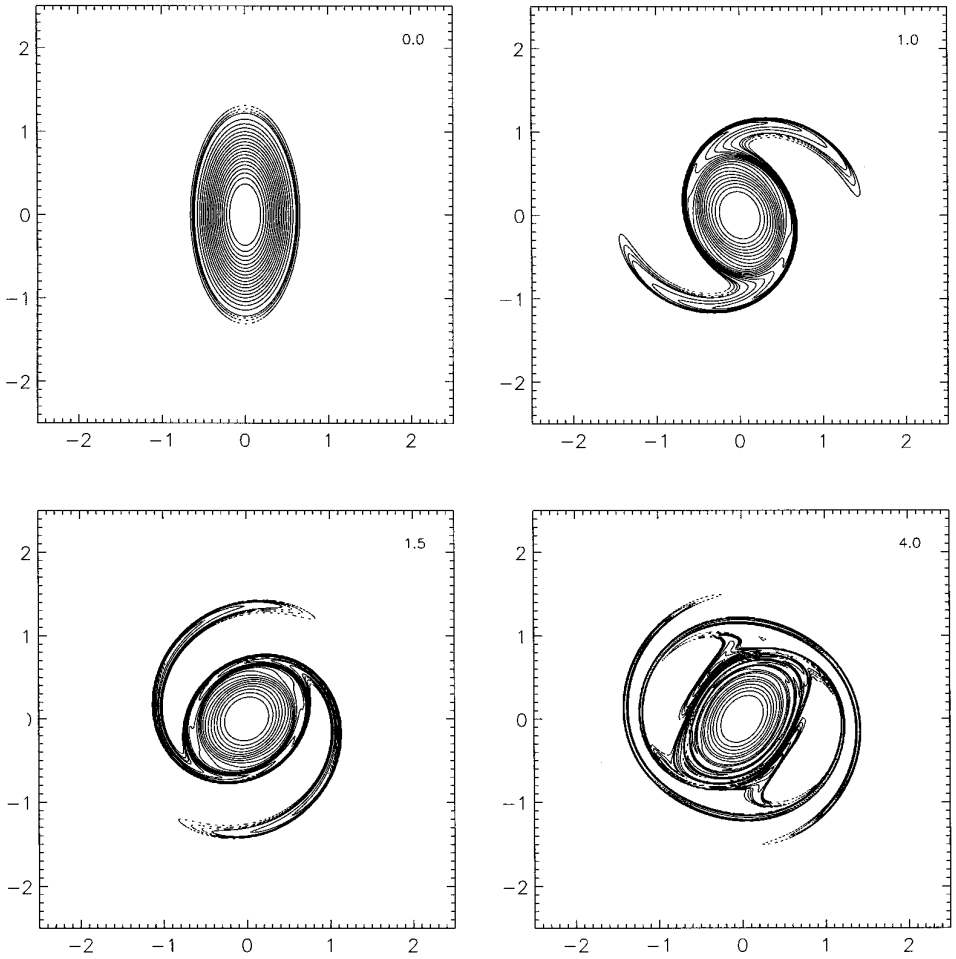


**FIG. 10.** Vorticity contours for the evolution of the vorticity fields ( $\omega^l$ ). Contours of 0.25, 0.50, 1, 2, ..., 20 at times 0, 1, 1.5, 4, 8, 12, 16, 24. Figures are ordered left to right, top to bottom. More detailed color contour plots may be viewed at the WWW address: <http://www.galcit.caltech.edu/~petros/RESEARCH/ellipse.html>.

to the vorticity core. Hyperviscosity, however, might have played a role in eliminating the radial gradients resolved by the present simulations. Moreover, the results of MMZ show a band of spurious negative vorticity surrounding the main vortex core (in the order of 5% of the maximum vorticity) and a respective reduction of the maximum vorticity. In the present results we may observe low amplitude, sharp gradients on the main vortex core as well as a more complex filamentary structure. Note that low amplitude (less than 0.05%) spurious negative vorticity was observed to develop on the periphery of the core in the present simulations as well. We believe, however, that due to its low amplitude it has had negligible effects on the evolution of the vortex.

The third stage of the evolution of the vorticity field ( $T \approx 7$  to  $T \approx 14$ ) is qualitatively similar to the second stage described above. The vortex core attracts



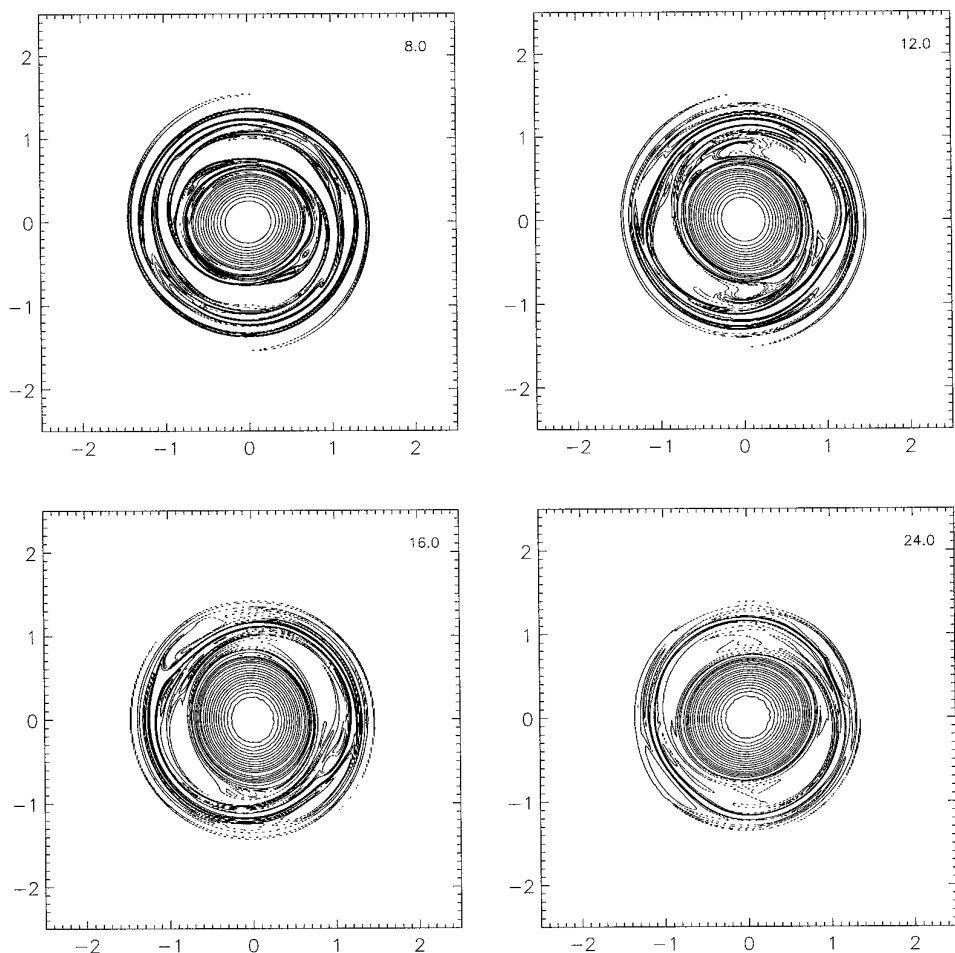
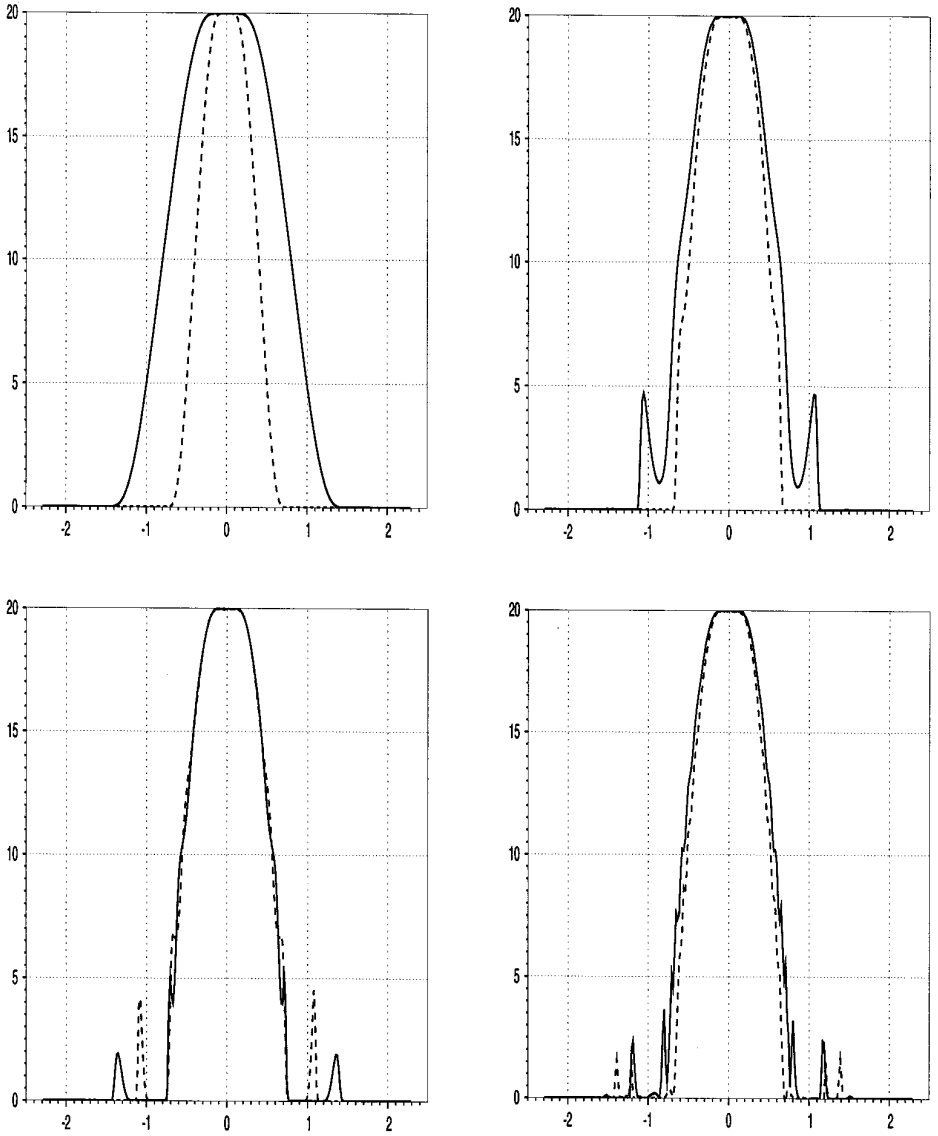


FIG. 10—Continued

some filamentary structures increasing its ellipticity and introducing again a weaker perturbation in the monotonicity of the vorticity profile. This is again followed by a new process of filamentation accompanied by a respective decrease of the ellipticity.

In the following stage ( $T \approx 14$  to  $T \approx 24$ ) this process seems to saturate and a stable axisymmetric configuration seems to be achieved consisting of a circular main vortex core surrounded by a spiraling disk of weak filamentary structures. The slight variations of the ellipticity observed at later times may be attributed to weak interactions of the vortex core with the filamentary structures. One may observe the spatial structure of the vorticity structure on the outer filaments resolved by the present computations. This resolution ensures that comparable vorticity gradients have not been smeared out on the vortex core by the present scheme and that the final stages of the simulation present a realistic picture of the asymptotic configuration.

Alternatively, Driscoll and Fine [6] demonstrated, via a stability analysis and related experiments, that axisymmetrization may be understood in terms of a reso-



**FIG. 11.** Vorticity profiles along  $x = 0$  (solid) and  $y = 0$  (dashed) of the vorticity field ( $\omega^j$ ) at  $T = 0, 1, 1.5, 4, 8, 12, 16, 24$ . Figures are ordered left to right, top to bottom.

nance between the perturbation wave and the fluid rotation at a critical radius where the vorticity is not spatially constant, giving rise to inviscid Landau damping of the wave [3]. When the resonant radius lies inside the vortex, damping will occur for small asymmetric distortions. This nonlinear damping may decrease or cease when the flow generates weak vortical filaments around the vortex core. Their analysis suggests that the critical radius for the present vorticity profile lies at  $\approx 0.89 R_0$ , justifying the observed axisymmetrization.

In Fig. 9 we present the energy spectrum of the vorticity field as computed by the present method. Note that most of the energy remains associated with the

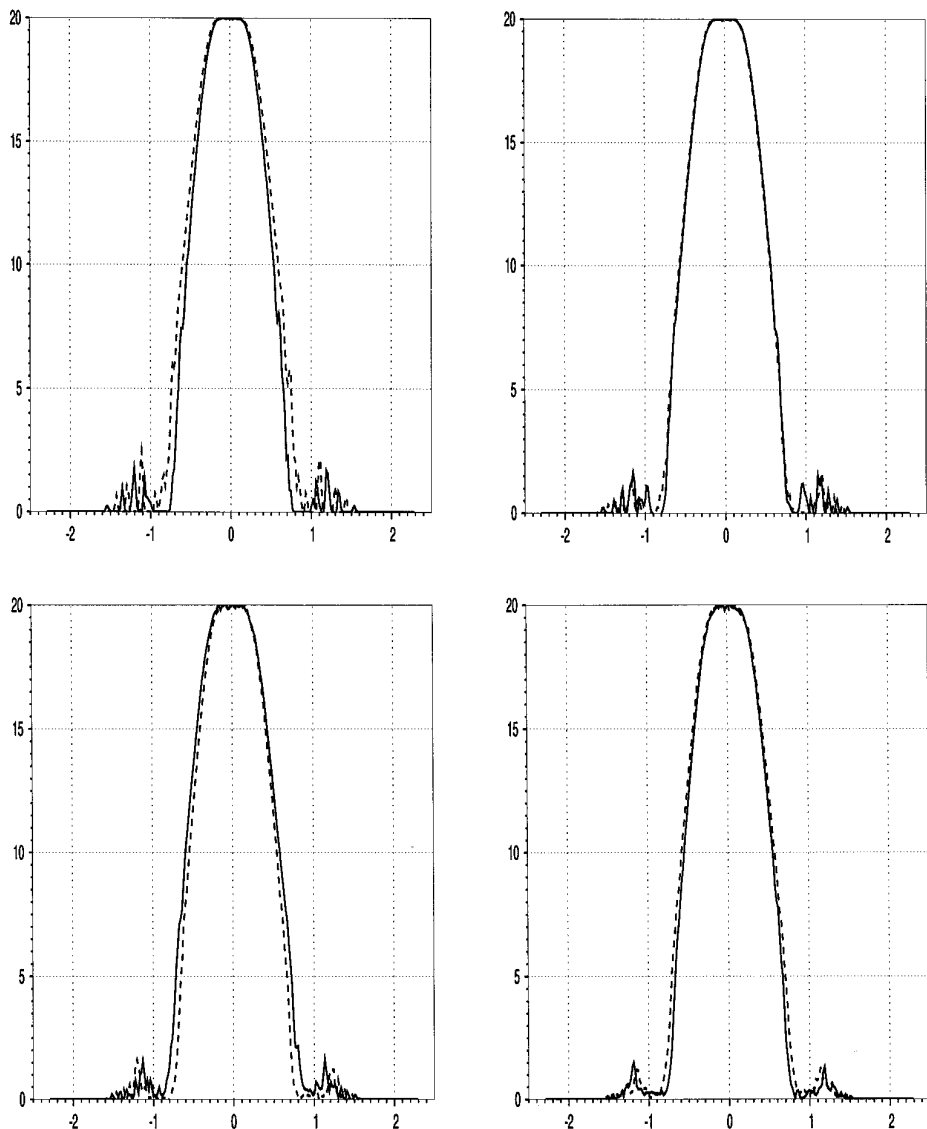
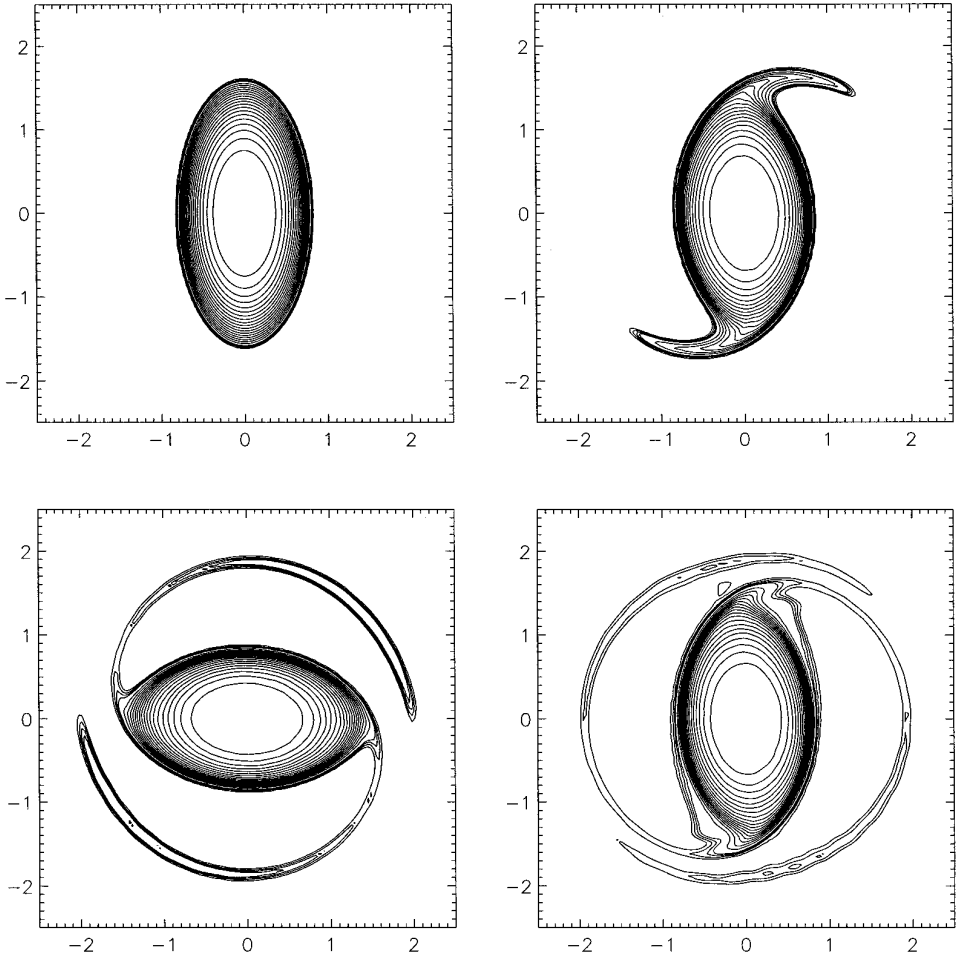


FIG. 11—Continued

vortex core. To further demonstrate the axisymmetrization of the vorticity profile we compare the final distribution with that of an idealized circular top-hat profile vortex having radius 0.6 and carrying 90% of the circulation of the total vorticity field (Fig. 9). Note that the high frequency oscillations correspond to the top-hat profile approximation and not to the filaments of the flow that appear to carry small amounts of energy.

### 5.2. Non-Axisymmetrization of $\omega^H$

In this case we may observe two major stages in the evolution of the elliptical vortex with the initial profile described by  $\omega^H$  (Fig. 12).



**FIG. 12.** Vorticity contours for the evolution of the vorticity field ( $\omega''$ ). Contours of 0.25, 0.50, 1, 2, ..., 20 at times 0, 1, 2, 4, 6, 12, 18, 24. Figures are ordered left to right, top to bottom.

In the first stage ( $T = 0$  to  $T \approx 4$ ) filamentation is initiated on the periphery of the vortex, resulting in two thin structures that undulate around the main core. The effective aspect ratio ( $\lambda_{\text{eff}}$ ) of the configuration (Fig. 8) initially decreases to 1.42, followed by a small increase as the filaments fold into a circular shape. Examining the vorticity profile (Fig. 13) one may observe a “kink” (a sharp change of the vorticity gradient) at the edges of the main vortex core. A second weaker filamentation process is then initiated, resulting in yet another decrease of the effective aspect ratio of the vortex structure.

This secondary filamentation interacts with the primary filaments, thus creating a link between the main vortex core and the peripheral structures. Repeated weaker filamentations appear to occur (e.g., see the profile at  $T = 18.0$ ) as the effective aspect ratio gradually asymptotes to a steady value of about 1.42 (close to the initial drop). The asymptotic structure of the configuration consists of a smooth *elliptical* core surrounded by a simple filamentary structure. Overall the evolution of the

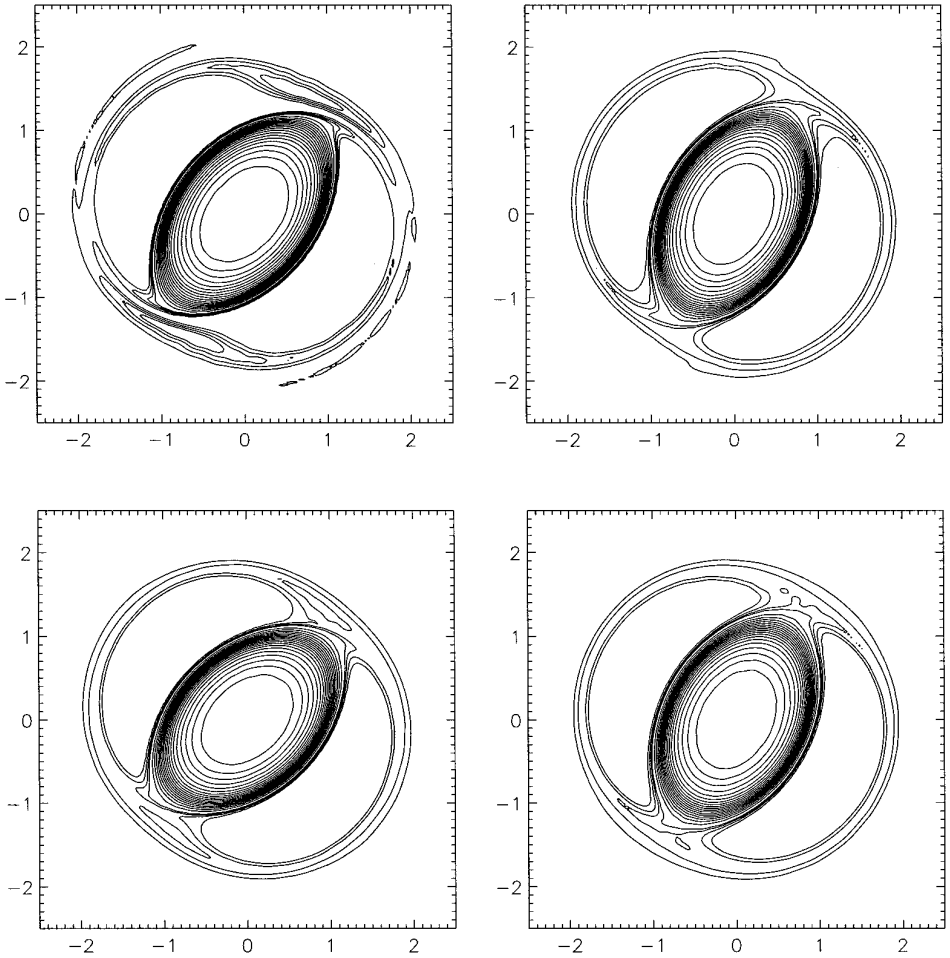
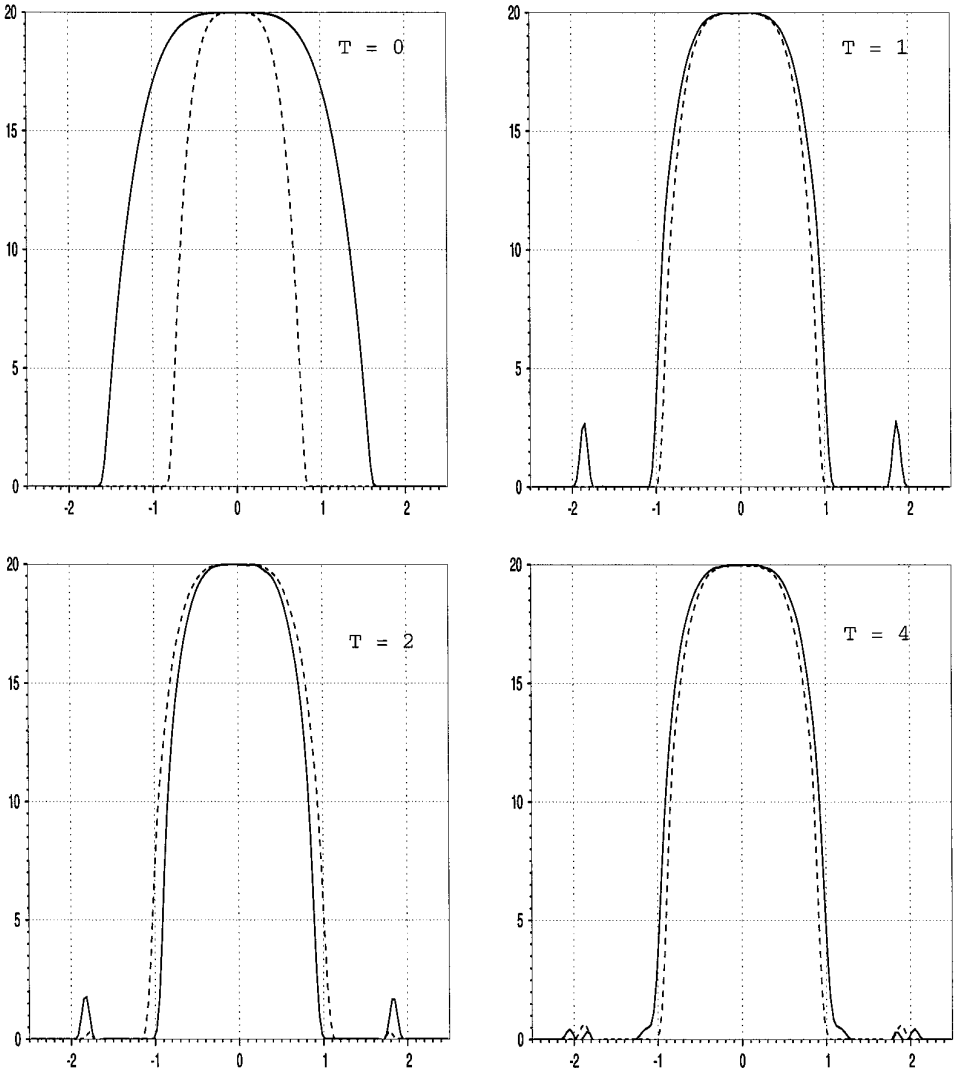


FIG. 12—Continued

vorticity field  $\omega^{II}$  exhibits a more quiescent filamentation process, compared to the repeated filamentations observed in the evolution of  $\omega^I$ . A comparison of the evolution of the vorticity profiles (Figs. 11 and 13) shows that, in the case of  $\omega^{II}$ , instabilities manifested as waves on the vortex core are limited at the outskirts of the vorticity field, hence the limited filamentation of the main robust elliptical vortex structure.

Dritschel [7] has observed a similar evolution for an eight-level piecewise vorticity distribution, which may be viewed as a stepwise approximation of the  $\omega^{II}$  profile. He observed a similar filamentation process and a similar evolution of the effective aspect ratio of the elliptical vortex. In his simulations there is an initial drop of  $\lambda_{\text{eff}}$  to a value of about 1.43 (in excellent agreement with the present results). However, after the initial drop there appears to be a discrepancy in the evolution of  $\lambda_{\text{eff}}$  compared with the results of the present simulations as  $\lambda_{\text{eff}}$  asymptotes towards a value of 1.70 (compared to 1.42 in the present simulations). This discrepancy may



**FIG. 13.** Vorticity profiles along  $x = 0$  (solid) and  $y = 0$  (dashed) of the vorticity field ( $\omega''$ ) at  $T = 0, 1, 2, 4, 6, 12, 18, 24$ . Figures are ordered left to right, top to bottom.

be attributed to the eight-level piecewise approximation of the profile  $\omega''$ . The piecewise vorticity field may evolve with/without secondary filamentation processes that correspond to filamentation processes of the respective continuous field. The number of levels in these approximations may be crucial, and a systematic study observing the evolution of the effective aspect ratio as a function of the levels of approximation of the vorticity structures could further elucidate this issue. Contour surgery simulations [17] have indeed demonstrated a consistent approximation of the evolution of continuous vorticity fields as the number of levels is increased.

Finally, in Fig. 16 we present a comparison of contours of the vorticity field from the present simulations equivalent to measurements of the charge density in pure

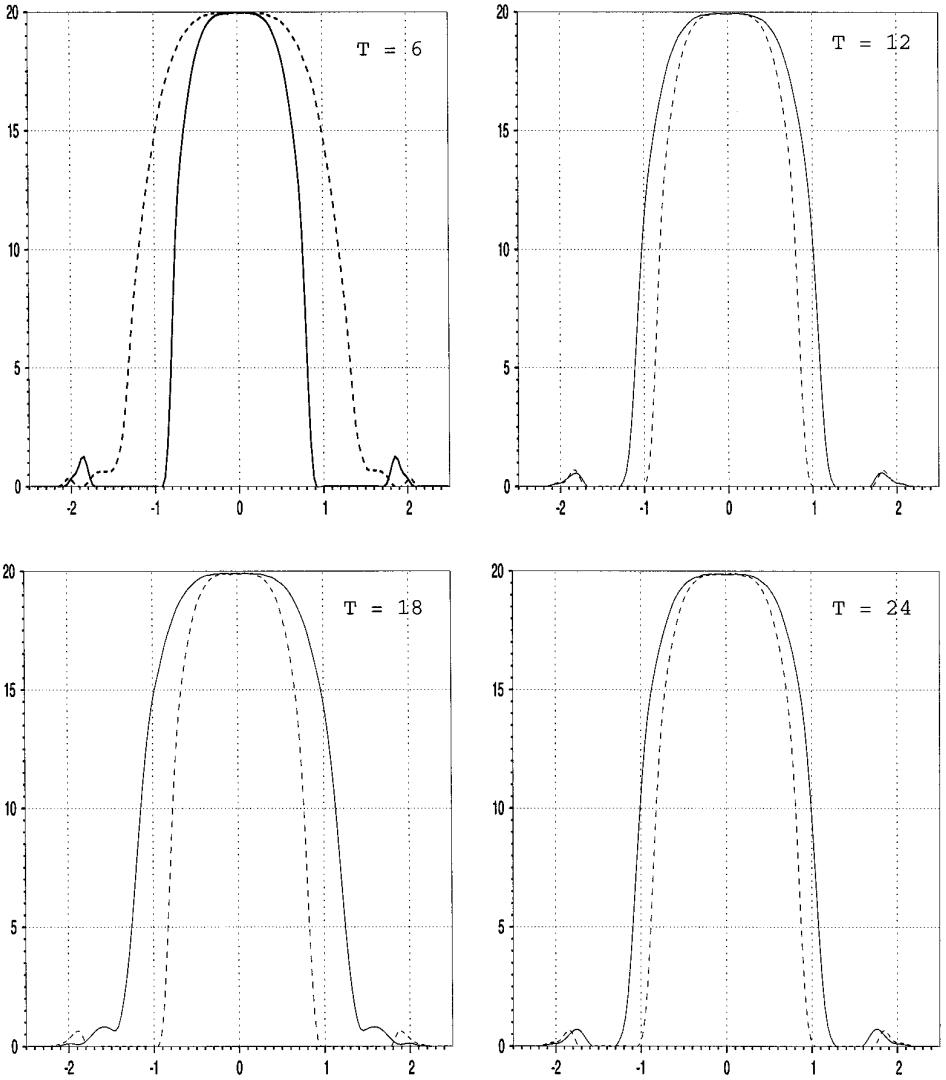


FIG. 13—Continued

electron plasmas [6] for a particular initial distribution. As the 2D drift Poisson equations governing the evolution of the magnetized electron column density are isomorphic to the Euler equations governing an inviscid vorticity field we can directly compare the two results. As discussed in Section 5.1, consider axisymmetrization as a result of a wave–fluid resonance. The occurrence and extent of this process depends on the strength of the vorticity at the resonant radius. For the present profile, their analysis places the critical radius at  $\approx 1.23R_0$ , well outside the vorticity distribution. This would imply the absence of any axisymmetrization. However, it appears that the differential rotation of the vorticity layers and the nonnegligible (2:1) aspect ratio of the ellipse resulted in transport of the vorticity outside this critical radius. The process saturates once the “Kelvin’s cat’s eyes” have formed,

resulting in a nonunity effective aspect ratio. The results of Driscoll and Fine clearly have demonstrated that the phenomenon of axisymmetrization depends on characteristics of the initial profile. The qualitative agreement with these results provides experimental validation to the results of the present simulations. Moreover, this agreement provides another independent confirmation that axisymmetrization is not a universal process for initially noncircular vortical structures.

### 5.3. Discussion

The present results indicate that the axisymmetrization of initially noncircular vortices depends on the shape of the initial vorticity profile. The minimal dissipation of the present simulations provide independent evidence for this phenomenon and complement the related computational works of Dritschel [7] (who first argued that this is a possible scenario) and MMZ [21], as well as the experimental works of Driscoll and Fine [6].

The initial reduction of the ellipticity of the vortex is attributed to the differential rotation of the layers of the smooth vorticity field. This rotation introduces a nonmonotonic vorticity profile susceptible to a Kelvin–Helmholtz-type of instability which is manifested as azimuthal vortical waves on the surface of the main vortex core. The vortex core has a stabilizing effect as it acts to stretch these vortex filaments, thus reducing their amplitude. The subsequent evolution of the vorticity field may be viewed as a nonlinear interaction of the vortex core with the filamentary structures. The magnitude of this reduction depends on size of the constant vorticity inner core and the sharpness of the vorticity gradients.

The analysis of Driscoll and Fine [6], describes the process of axisymmetrization as a nonlinear damping due to the direct resonance of the core vorticity with the fluid rotation at a critical radius. This analysis is consistent with the results presented herein and by MMZ as it suggests that the resulting axisymmetric state is the result of resonance at the critical radius of the particular initial vorticity profile. Moreover, it does not preclude the possibility of asymptotic nonaxisymmetric configurations, as for vorticity profiles that are “sufficiently” sharp the critical radius may lie completely outside the vortex, in which case no resonant damping is observed. In this case, for certain values of the ellipticity, weak outer vorticity layers (corresponding to “electrons that become resonant with the wave,” as described in [6]) are shed from the vortex and eventually form the stable weak filamentary structures observed in experiments and computations (Fig. 16). This behavior is consistent with the evolution of a sharper vorticity profile described by earlier CS simulations. Care must be exercised, however, as to the interpretation of nonsharp edged profiles approximated by piecewise vorticity distributions, as such an idealization may preclude this resonance in general [14] and/or may lead to asymptotic structures that differ from the respective continuous vorticity fields that they approximate.

The present results demonstrate that the initial profile determines the crucial initial reduction of the eccentricity of the vortex. These initial stages of the evolution may be handled efficiently and accurately by all numerical schemes discussed herein. However, the accurate description of the long-time evolution presents a challenge to the particulars of each scheme. In vortex methods a lower spatial resolution



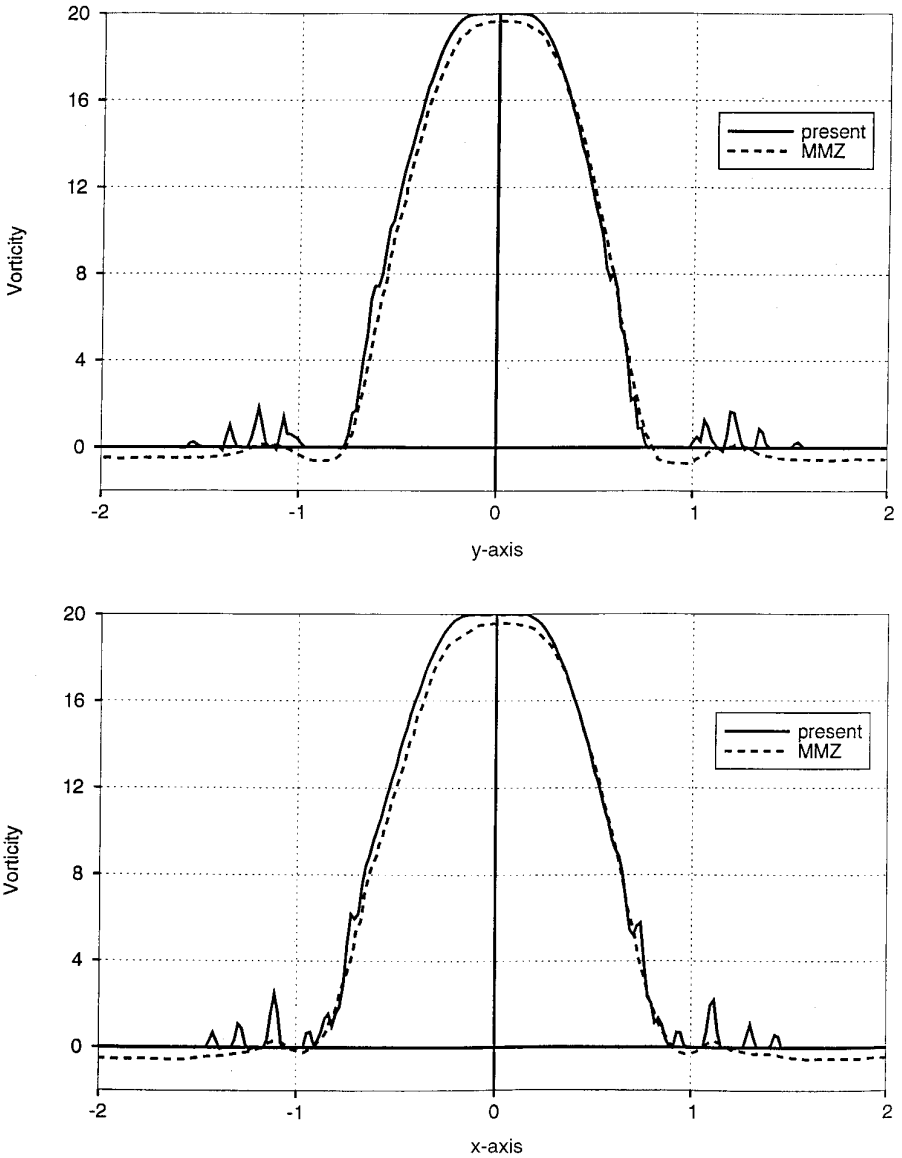


**FIG. 14.** Comparison of the results of the present simulations with the results of MMZ at  $T = 8$ . Vorticity profiles.

could damp the waves developing on the vortex core and reduce the phenomenon of axisymmetrization, but on the other hand, this additional dissipation may lead to the weakening of the filamentary structures, thus not allowing us to properly resolve their interaction with the vortex core at the later stages of the evolution of the ellipse. Hyperviscous pseudospectral simulations may lead to the generation of unphysical vorticity structures while suppressing sharp vorticity gradients. As vorticity gradients are the driving mechanism of the evolution of inviscid two-dimensional flows [1] one needs to be skeptical about the results of such simulations. Contour

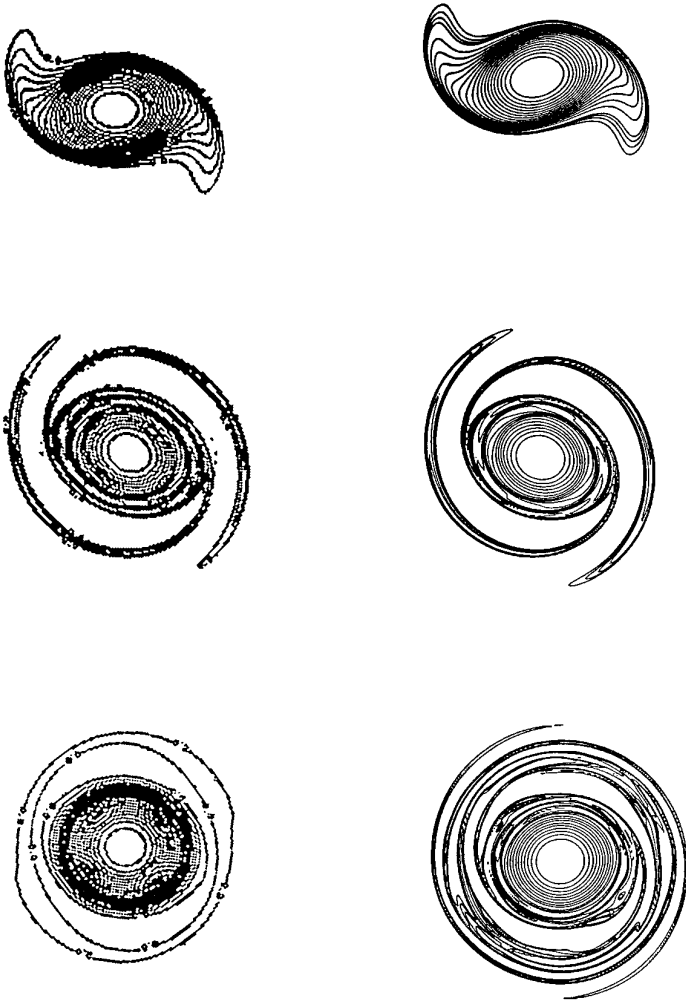
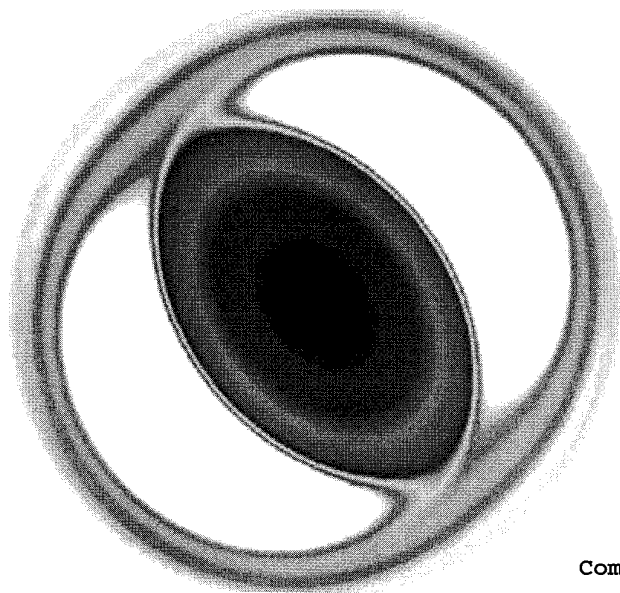
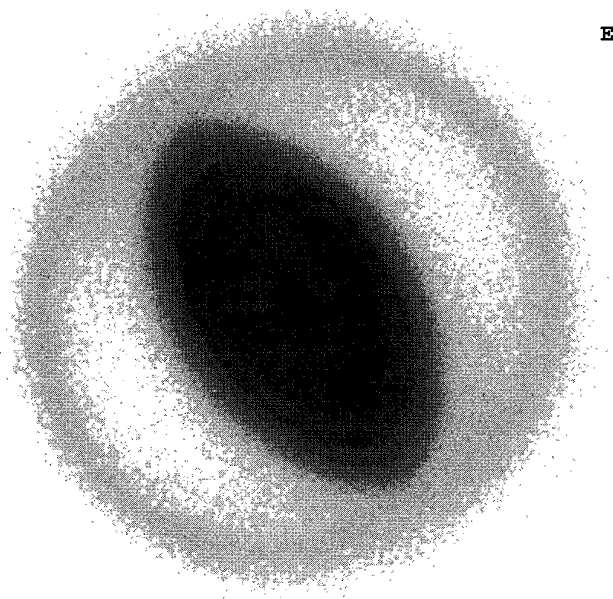


**FIG. 15.** Comparison of the results of the present simulations with the results of MMZ at  $T = 8$ . Vorticity contours.

surgery simulations seem to accurately resolve the azimuthal gradients observed in the vortical structures described above, given enough resolution. Some questions arise, however, as the piecewise approximation of a continuous vorticity profile with a limited number of constant vorticity steps may inhibit certain instabilities [14] of the vorticity field and suppress/enhance filamentation processes present/absent in continuous vorticity distributions. These observations may affect predictions regarding population dynamics of general vortical fields at the inviscid limit [13] and one must carefully take into consideration the details of the numerical scheme used to obtain such information.

Finally, based on the observations made in these simulations and in simulations involving contour dynamics, a new methodology for long-time highly accurate simulations of inviscid flows involving vortical structures with sharp vorticity gradients

## Experiments



## Computations

**FIG. 16.** Comparison of the asymptotic state of the present simulations (b) with the results (a) of Driscoll and Fine [6].

may be proposed. Such a scheme would be a hybrid of contour dynamics and high resolution vortex methods. The inner, rather uniform part of the vortex, would be approximated by a few piecewise continuous distributions of vorticity, whereas regions of high vorticity gradients would be approximated by vortex methods. As the inner part of the vorticity does not develop high gradients a simple contour

dynamics procedure would suffice. Such a hybrid method is easy to formulate as a composition of complementing Lagrangian methods and would reduce the computational cost involved in vortex dynamics simulations, as very few computational elements would be used to describe the inner part of vorticity field. Moreover, the fast algorithms employed herein for the advancement of particles could be easily extended to account for the velocity field induced by the boundary elements employed in the discretization using contour dynamics. Work is under way to implement this methodology in the study of population dynamics of vortical structures with sharp gradients.

## 6. CONCLUSIONS

A high resolution Lagrangian numerical method for the simulation of the inviscid evolution of smooth vortical structures, is presented. A convergence study demonstrates that the present method can be implemented for accurate long time simulations of inviscid vortical flows, offering a viable alternative to schemes such as pseudo-spectral methods and contour surgery.

The method is applied to the study of the phenomenon of inviscid axisymmetrization of initially elliptical vorticity distributions. Long-time, high resolution simulations reveal that axisymmetrization may or may not occur, depending on the shape of the initial vorticity field. We discuss the evolution of the vorticity field and we compare our results with related computational and experimental works.

## ACKNOWLEDGMENTS

I thank Professor Fred Driscoll and Ms. Ann Cass of UCSD for many enlightening discussions, as well as for kindly providing me with an original picture from their work. Computer time was provided by NASA Ames.

## REFERENCES

1. G. K. Batchelor, Computation of the energy spectrum in homogeneous two-dimensional turbulence, *Phys. Fluids Suppl.* **2**, 233 (1969).
2. J. T. Beale, On the accuracy of vortex methods at large times, in *Proc. Workshop on Comput. Fluid Dyn. and React. Gas Flows, IMA, Univ. of Minnesota, 1986*.
3. J. R. Briggs, J. D. Daugherty, and R. H. Levy, Role of Landau damping in cross-field electron beams and inviscid shear flow, *Phys. Fluids* **13**, 421 (1970).
4. A. J. Chorin, Numerical study of slightly viscous flow. *J. Fluid Mech.* **57**, 380 (1973).
5. J. P. Christiansen, Vortex methods for flow simulation. *J. Comput. Phys.* **13**, 363 (1973).
6. C. F. Driscoll and K. S. Fine, Experiments on vortex dynamics in pure electron plasmas. *Phys. Fluids B* **6**, 1359 (1990).
7. D. G. Dritschel, Contour dynamics and contour surgery: numerical algorithms for extended, high-resolution modelling of vortex dynamics in two dimensional, inviscid, incompressible flows. *Comp. Phys. Rep.* **10**, 77 (1989).
8. K. S. Fine, A. C. Cass, W. G. Flynn, and C. F. Driscoll, Relaxation of 2D turbulence to vortex crystals.
9. D. Gottlieb and S. A. Orszag, *Numerical Analysis of Spectral Methods: Theory and Applications* (SIAM, Philadelphia, 1977).

10. L. Greengard and V. Rokhlin, A fast algorithm for particle simulations. *J. Comput. Phys.* **73**, 325 (1987).
11. O. H. Hald, Convergence of vortex methods for Euler's equations II. *SIAM J. Numer. Anal.* **16**, 726 (1979).
12. R. W. Hockney and J. W. Eastwood, *Computer Simulation Using Particles*. McGraw-Hill, New York, 1981.
13. J. Jiménez, Hyperviscous vortices. *J. Fluid Mech.* **279**, 169 (1994).
14. Kelvin, W. On a disturbing infinity in Lord Rayleigh's solution for waves in a plane vortex stratum. *Nature* **23**, 45 (1880).
15. P. Koumoutsakos, *Direct Numerical Simulations of Unsteady Separated Flows Using Vortex Methods*, Ph.D. thesis, California Institute of Technology, 1993.
16. P. Koumoutsakos and A. Leonard, High-resolution simulations of the flow around an impulsively started cylinder using Vortex Methods. *J. Fluid. Mech.* **296**, 1 (1995).
17. B. Legras and D. Dritschel, A comparison of the contour surgery and pseudo-spectral methods. *J. Comput. Phys.* **104**, 287 (1993).
18. A. Leonard, Vortex methods for flow simulation. *J. Comput. Phys.* **37**, 289 (1980).
19. A. Leonard, Calculation of the energy spectrum in vortex methods, private communication, 1989.
20. A. Mariotti, B. Legras, and D. Dritschel, Vortex stripping and the erosion of coherent structures in two-dimensional flows. *Phys. Fluids* **6**, 3954 (1994).
21. J. C. Melander, J. C. McWilliams, and N. J. R. Zabusky, Axisymmetrization and vorticity-gradient intensification of an isolated two-dimensional vortex through filamentation. *J. Fluid Mech.* **178**, 137 (1987).
22. T. B. Mitchell and C. F. Driscoll, Symmetrization of 2D vortices by beat-wave damping. *Phys. Rev. Letters* **73**, 2196 (1994).
23. J. J. Monaghan, Particle methods for hydrodynamics. *Comp. Phys. Reports* **3**, 71 (1985).
24. D. I. Pullin, Contour dynamics methods. *Ann. Rev. Fluid Mech.* **24**, 89 (1992).
25. J. W. S. Rayleigh, On the stability, or instability, of certain fluid motions. *Proc. London. Math. Soc.* **11**, 57 (1880).
26. L. Rosenhead, The formation of vortices from a surface of discontinuity. *Proc. Roy. Soc., Ser. A* **134**, 170 (1931).
27. I. J. Schoenberg, *Cardinal Spline Interpolation*. SIAM, Philadelphia, 1973.
28. G. Winckelmans and A. Leonard, Contributions to vortex particle methods for the computation of three and two-dimensional incompressible unsteady flows. *J. Comp. Phys.* **109**, 247 (1993).
29. H. B. Yao, N. J. Zabusky, and D. G. Dritschel, High gradient phenomena in two-dimensional vortex interactions. *Phys. Fluids* **7**, 539 (1995).
30. N. J. Zabusky, M. H. Hughes, and K. V. Roberts, Contour dynamics for the Euler equations in two dimensions. *J. Comput. Phys.* **30**, 96 (1979).